



THE UNIVERSITY *of* EDINBURGH

## Edinburgh Research Explorer

# Mixed Carbonate–Siliciclastic Sedimentation Along the Great Barrier Reef Upper Slope: A Challenge To the Reciprocal Sedimentation Model

### Citation for published version:

harper, B, PUGA-BERNABEU, ANGEL, droxler, A, Webster, J, Gischler, E, Tiwari, M, lado-insula, T, Thomas, A, morgan, S, jovane, L & ROHL, URSULA 2015, 'Mixed Carbonate–Siliciclastic Sedimentation Along the Great Barrier Reef Upper Slope: A Challenge To the Reciprocal Sedimentation Model', *Journal of Sedimentary Research*, vol. 85, no. 9, pp. 1019. <https://doi.org/10.2110/jsr.2015.58.1>

### Digital Object Identifier (DOI):

[10.2110/jsr.2015.58.1](https://doi.org/10.2110/jsr.2015.58.1)

### Link:

[Link to publication record in Edinburgh Research Explorer](#)

### Document Version:

Peer reviewed version

### Published In:

Journal of Sedimentary Research

### General rights

Copyright for the publications made accessible via the Edinburgh Research Explorer is retained by the author(s) and / or other copyright owners and it is a condition of accessing these publications that users recognise and abide by the legal requirements associated with these rights.

### Take down policy

The University of Edinburgh has made every reasonable effort to ensure that Edinburgh Research Explorer content complies with UK legislation. If you believe that the public display of this file breaches copyright please contact [openaccess@ed.ac.uk](mailto:openaccess@ed.ac.uk) providing details, and we will remove access to the work immediately and investigate your claim.



**MIXED CARBONATE-SILICICLASTIC SEDIMENTATION ALONG THE GREAT  
BARRIER REEF UPPER SLOPE: A CHALLENGE OF THE RECIPROCAL  
SEDIMENTATION MODEL**

BRANDON B. HARPER<sup>1\*</sup>, ÁNGEL PUGA-BERNABÉU<sup>2,3</sup>, ANDRÉ W. DROXLER<sup>1</sup>, JODY  
M. WEBSTER<sup>3</sup>, EBERHARD GISCHLER<sup>4</sup>, MANISH TIWARI<sup>5</sup>, TANIA LADO-INSUA<sup>6</sup>,  
ALEX L. THOMAS<sup>7</sup>, SALLY MORGAN<sup>8</sup>, LUIGI JOVANE<sup>9</sup>, and URSULA RÖHL<sup>10</sup>

<sup>1</sup>*Department of Earth Science, Rice University, Houston, Texas, 77005, U.S.A.*

<sup>2</sup>*Departamento de Estratigrafía y Paleontología, Universidad de Granada, Granada, 18002, Spain*

<sup>3</sup>*Coastal Research Group, School of Geosciences, The University of Sydney, NSW 2006, Australia*

<sup>4</sup>*Institut für Geowissenschaften, Goethe-Universität, 60438 Frankfurt am Main, Germany*

<sup>5</sup>*National Centre for Antarctic and Ocean Research, Vasco-da-Gama 403 804, India*

<sup>6</sup>*Graduate School of Oceanography, University of Rhode Island, Narragansett, Rhode Island, 02882,  
U.S.A.*

<sup>7</sup>*School of Geosciences, University of Edinburgh, Edinburgh EH9 3JW, United Kingdom*

<sup>8</sup>*Borehole Research Group, Lamont-Doherty Earth Observatory of Columbia University, Palisades,  
New York, 10964, U.S.A.*

<sup>9</sup>*Instituto Ocenográfico, Universidade de São Paulo, São Paulo 05508-120, Brazil*

<sup>10</sup>*MARUM - Center for Marine Environmental Sciences, Universität Bremen, D-28334 Bremen,  
Germany*

*\*email:brandon.b.harper@rice.edu*

## ABSTRACT

Results of studies involving numerous cores and ODP holes along the Great Barrier Reef (GBR) margin and adjacent Queensland Trough and Queensland Plateau have challenged the use of a reciprocal sedimentation model to describe the sedimentary response of slope and basin settings to glacioeustatic sea level fluctuations. Upper slope sedimentation results from the relationships between sea-level fluctuations, antecedent topography, and regional climate that play an important role in the type and amount of sediment deposited on the upper slope during glacial, deglacial, and interglacial times. During the Last Glacial Maximum (LGM, > 20 ka ago) upper slope sediments generally lacked siliciclastic material and are characterized by very low accumulation rates, whereas early deglacial-time (Termination I, TI) deposits are dominated by a siliciclastic and neritic carbonate pulse. Siliciclastic sedimentation was significantly reduced in the Holocene, while carbonate sedimentation remains elevated. A new borehole, IODP Expedition 325 Hole M0058A (Hole 58A), recovered 82% of a 40.4 m hole on the upper slope east of Noggin Passage on the central GBR margin near Cairns, Australia. Hole 58A provides a detailed sedimentary record during Termination II (TII), Marine Isotope Stage 6/5e (MIS-6/5e), deglacial transition, and through most of interglacial MIS-5. This hole, along with two others (ODP Leg 133 Holes 820A and 819A from the upper slope east of Grafton Passage), show carbonate-siliciclastic cyclicity as the result of glacioeustatic change with the GBR shelf. Sedimentation at Hole 58A is consistent with that of previous studies along the GBR margin (focusing on the LGM to present), and extends the upper slope sedimentary record back to TII and interglacial MIS-5. A siliciclastic pulse similar to the one during TI occurred during the penultimate deglaciation, TII; however, the maximum neritic aragonite export to the upper slope occurred not during peak MIS-5e highstand when sea level was a few meters above modern

position, but subsequently during a time (MIS-5d to 5a) when lowered sea level fluctuated between 30 and 50 m below present sea level. Siliciclastic sediments were reworked and exported to the upper slope when the lowstand fluvial plain was re-flooded, whereas neritic carbonate export to the slope reaches a maximum when sea level fell and much of the mid to outer shelf re-entered the photic zone, subsequent to a drowning interval. Thus, this analysis refines the mixed sedimentation models of upper slope sedimentation along the central GBR margin during the penultimate deglacial transgression and subsequent interglacial early and late highstand. This study provides further evidence that mixed carbonate-siliciclastic margins do not always behave in a predictable manner and that mixed margins both modern and ancient would benefit from detailed study of sediment transport in the context of sea level rise and fall.

## INTRODUCTION

Low latitude mixed carbonate-siliciclastic depositional systems occur globally where tropical neritic environments line continental shelf edges. Major mixed systems are found today in northeast Australia and Papua New Guinea (Davies et al. 1989; Tcherepanov et al. 2008), Panama (McNeill et al. 2013) as well as Belize (Esker et al. 1998; Ferro et al. 1999; Purdy and Gischler 2003; Gischler et al. 2010). Sedimentation on the modern upper slope of the central Great Barrier Reef (GBR) margin comes from carbonates (*in situ* benthic species, pelagic foraminifers and pteropods, and transported neritic fine and coarse detritus) and siliciclastics (transported fine silts and clays, Harris et al. 1990; Dunbar et al. 2000; Francis et al. 2007). Areas in close proximity to reefs record intervals of exposure and calcium carbonate production with the accumulation of fine neritic sediments (Dunbar et al. 2000). Upper slope sediments may be reworked and redistributed by physical processes such as currents, tides, and sediment

density flows. The relatively smooth uppermost slope is typically free of gravity flow erosion, whereas the gullied deeper slope areas and locations such as the Ribbon Reefs are more prone to erosion by sediment gravity flows (Dunbar et al. 2000; Webster et al. 2012; Puga-Bernab   et al., 2014).

Mixed carbonate-siliciclastic systems have been described by the reciprocal sedimentation model, often based on ancient examples from outcrop: the maximum and minimum mass accumulation rates (MAR) of siliciclastic material to the upper slope occurring during sea level lowstand and highstand, respectively, whereas maximum carbonate sediment delivery to the upper slope occurs during sea-level highstand (Wilson 1967; Sarg 1988; Dolan 1989; Handford and Loucks 1993; Schlager et al. 1994). This model has been challenged and shown to be inadequate for describing GBR margin sedimentation rates by several studies focusing on the last glacial-interglacial transition along the GBR margin (Peerdeman and Davies 1993; Dunbar et al. 2000; Dunbar and Dickens 2003a; Dunbar and Dickens 2003b, Page et al. 2003; Page et al. 2005; Francis et al. 2007; Bostock et al. 2009; Webster et al. 2012). These studies found that during the Last Glacial Maximum (LGM) lowstand, siliciclastic and carbonate sedimentation rates were consistently low from the slope into the basin. However, during late transgression (Termination I, TI), siliciclastic and carbonate sedimentation rate increased dramatically on the upper slope, and declined to near lowstand rates within the Queensland Trough. During the Holocene interglacial, highstand siliciclastic sediment accumulation rate declined, whereas carbonate sedimentation remained elevated (highstand shedding) along the slope.

The highstand shedding concept is a response of carbonate platforms to sea level flooding and highstand conditions (Schlager and Chermak, 1979; Boardman and Neumann, 1984;

Droxler et al., 1985; Grammer and Ginsburg 1992; Schlager et al., 1994; Betzler et al. 2000; Slowey et al., 2002; Andresen et al. 2003; Jorjy et al. 2010; Paul et al. 2012). Although the highstand shedding concept is consistent with Holocene sediment accumulation along the GBR margin, neritic carbonate accumulation and export appear to have been already initiated during the late transgression (Dunbar et al. 2003b; Page et al. 2005; Jorjy et al. 2010). Neritic carbonate production and export can also be triggered when sea level on a carbonate platform, drowned during a relative sea level highstand, starts to fall (Droxler et al. 1993).

The aim of this study is to characterize the mixed carbonate-siliciclastic sediment record along the central GBR margin during the penultimate deglacial and interglacial time as an example of mixed system sea level response that is not consistent with the reciprocal sedimentation model. Mixed carbonate-siliciclastic systems have been common throughout the geologic past (Dorobek 2008); however, few outside of the GBR and Belize have been studied in the context of well-established sea level curves. In almost all cases, with the exception of the Late Pliocene Queensland Plateau (Droxler et al. 1993), postulated for some Campanian-Maastrichtian deposits (Shanmugam and Moiola 1983), and Early Cretaceous platform in the French Alps (Jacquin et al. 1990), the presence of carbonates is assumed to be the result of highstand shedding and a reflection of a period of elevated sea level (Schlager et al. 1994). This is, however, a potentially false assumption as this study of the central GBR shows. Chronologic, compositional, and sedimentological analysis of upper slope long sediment cores: IODP Expedition 325 Hole M0058A (Hole 58A), in conjunction with ODP Leg 133 Holes 819A and 820A on the central GBR, as well as piston core MD05-2949 (MD-49) on the northern GBR margin are used together published sea level curves to test the reciprocal sedimentation model, the concepts of transgressive siliciclastic shedding (Dunbar et al. 2000; Dunbar and Dickens

2003a; Page and Dickens 2005) and highstand carbonate shedding (Schlager et al. 1994). Additionally, carbonate shedding has been shown to cease when the bank-top is exposed during sea level fall, resulting in the shut off or large reduction of neritic carbonate on the adjacent slopes such as in the Gulf of Papua (Jorjy et al. 2010), Maldives (Paul et al. 2012), Caribbean (Jorjy et al., 2010), Bahamas (Droxler and Schlager 1985), and other locations globally in the Pliocene and Quaternary (Schlager et al. 1994).

The results of this study show that siliciclastic sedimentation is consistently follows the transgressive shedding model along the GBR during TI and TII; however, carbonate off-bank transport in relation to sea level fluctuations is highly variable not only between TI to MIS-1 and TII to MIS-5, but also from north to south along the GBR margin. If “highstand shedding” so variable along the GBR margin spatially and temporally, it stands to reason that other mixed systems may experience variability. Variability that is missed if highstand shedding alone is assumed. Furthermore, when sea level is poorly constrained and the presence and lack of neritic carbonate on slopes is used to identify periods of time when the bank is flooded and then exposed (respectively), the alternative of drowning (lack of carbonate) and photic zone re-entry during sea level fall (presence of carbonate) is often neglected. Finally, this study also serves as a modern analog for ancient mixed systems that appeared to not fit the concepts of highstand shedding and reciprocal sedimentation.

## STUDY AREA

The GBR margin is ~2,500 km long extending in latitudes from 9.5° S to 24.5° S (Fig. 1). The majority of the GBR lies offshore the northeastern coast of Australia, mostly along the Queensland continental middle shelf and shelf edge with some reefs located in coastal fringing

environments. In contrast, along the most northern extremity, reefs line the eastern side of the Torres Strait within the Gulf of Papua (GoP). The Queensland shelf is ~250 km at its widest near 21° S and narrows markedly north of Cairns to only ~50 km. From the Queensland shelf edge, the sea floor deepens towards the east into the Queensland Trough. In the GoP, the GBR bounds a broader ~150 km-wide shelf that deepens into the Ashmore Trough east of the Torres Strait (Francis et al. 2008; Tcherepanov et al. 2008). The Ashmore Trough is bounded on its northern and eastern sides by three isolated carbonate platforms (Ashmore, Boot, and Portlock atolls) and on its western side by the northern extremity of the GBR. Tropical monsoonal high precipitation climate coupled with very high topographic relief generate  $1.7 \times 10^9$  tons of sediment discharged annually by the Fly River, making up more than half of the sediment discharged by the rivers draining into the GoP (Milliman 1995). Conversely, high rainfall near Cairns, Australia, leads to high riverine discharge, however this runoff is associated with low sediment loads due to the extensive plant cover and low topographic relief of the uplands flanking the northern Queensland continental shelf (Gagan et al. 1987; Neil et al. 2002).

This study focuses on dataset samples collected from the site of Hole 58A and published datasets from Hole 819A (Davies et al. 1991), Hole 820A (Peerdeman and Davies 1993), and MD-49 (Jorjy et al. 2010). Hole 58A is located on the upper slope of the central GBR east of Noggin Passage (146° 35.357' E, 17° 5.8356' S) at a water depth of 170.31 m, ~1 km from the shelf edge (Figs. 1A and 1B). Hole 58A was drilled to a depth of 41.40 mbsf and recovered 33.94 m of sediment (81.98% recovery). ODP Leg 133 Holes 820A/B and 819A are located along a transect on the upper slope of the GBR east of Grafton Passage (146° 18.229' E, 16° 38.221' S and 146° 19.486' E, 16° 37.439' S) at water depths of 280.6 m and 565.2 m, respectively (Fig. 1A and 1B). Piston core MD05-2949 (MD-49) is located at the northern



extent of the GBR within the GoP, on Ashmore Trough upper slope (144°79.82'E, 10°04.07'S),  
at water depth of 657 m (Fig. 1A and 1C).

## SAMPLES AND METHODS

A total of 319 core samples were collected in 2 cm thick slabs, taken at 10 cm intervals  
down Hole 58A. These samples were analyzed for grain size, carbonate content, light  
reflectance, physical properties (Webster et al. 2011), elemental composition by X-ray  
fluorescence (XRF) analysis, and stable oxygen isotopes. In addition, 63 samples from Hole  
58A were collected every 50 to 100 cm and analyzed for mineralogy by X-ray diffraction  
(XRD).

The following steps were conducted in the systematic sample analytical preparation. Six  
grams of material were taken from each sample for detailed laser particle size analysis.  
Subsequently samples were oven-dried at 70°C for 24 hours and then weighed to obtain dry  
weight. Dried samples were placed in a phosphate-buffered solution (pH 7.5) for 24 hours and  
then washed over a 63 µm sieve to separate fine fraction (< 63 µm) from coarse fraction (> 63  
µm). The coarse size fraction was oven-dried at 70°C and then weighed and subtracted from the  
bulk sample to determine coarse- and fine-grained sediment percentages. The fine fraction was  
settled out in a 2000 mL beaker, dried, and collected for carbonate content analysis. The dried  
coarse fraction was split and sieved with a 250 and 300 µm screen.

The portion separated between 250 and 300 µm was examined using a Wild Heerbrugg  
stereomicroscope for the extraction of twenty to twenty-five *Globigerinoides ruber* (*G. ruber*)  
(white) specimens for stable isotope analysis and foraminiferal biostratigraphy. Once picked,  
each sample was placed in a small glass vial, filled partially with methanol and placed in a

sonicator for 8 seconds to remove fine sediment that might have adhered to the foraminiferal tests. The foraminifera were then placed in another glass vial and sent for stable isotope (oxygen, carbon) analysis using a GV Instruments Optima mass spectrometer. The isotope values are reported relative to V-PDB in delta notation with an analytical precision of  $\pm 0.04\%$ .

Downhole variations of oxygen stable isotopes of planktic foraminifera in Hole 58A were compared with the LR04 stacked record of Lisiecki and Raymo (2005), and served as the main basis to establish a detailed chronology in Hole 58A. Sea surface temperatures did not change in the western Coral Sea more than  $\sim 1.5^{\circ}\text{C}$  over the last  $\sim 800$  ky between glacial and interglacial stages (Lawrence and Herbert 2005), and thus the planktic oxygen isotope variations mostly records ice sheet accumulation and ablation and, therefore, a proxy for sea-level change related ice volume change.

Six AMS radiocarbon dates were obtained, out of which three were beyond the radiocarbon dating limits (see methods in Linick et al. 1986). The dates were obtained on selected species of planktic foraminifera (*G. ruber*, *G. sacculifer*, and *N. dutertrei*; size range: 250-420  $\mu\text{m}$ ; each sample sent to the AMS lab weighed around 10 mg) because sufficient foraminifera from a single species were not present to carry out monospecific dating (Linick et al., 1986). The radiocarbon ages were calibrated via the program CALIB 7.0.2 (Reimer et al. 2013) with a reservoir age correction of  $400 \pm 13$  years using the 'Marine13' calibration curve. The Marine Isotope Stage 6-5e transition ( $\sim 125$  ka) was identified by the systematic disappearance of pink-pigmented *G. ruber* as it occurs in Indo-Pacific cores (Thompson et al. 1979). Archives of core sections from Hole 58A were run through a XRF core scanner for rapid non-destructive chemical composition analysis. Hole 58A cores were scanned using an AVAATECH Scanner (Areva Group). The core surface was smoothed and coated with a 6  $\mu\text{m}$

polypropylene film to avoid drying of the core and contamination of the XRF scanner.

Elemental composition data were collected every 1 cm and only down core variations of Strontium (Sr) and Silica (Si) are presented in this study.

Sixty samples in Hole 58A were selected and analyzed for mineralogy (carbonates and non-carbonates) using XRD. All XRD measurements were performed on a Philips X'Pert Pro MD X-ray diffractometer equipped with a Cu tube ( $K\alpha$ ,  $\lambda$  1.541), 15-sample changer, secondary monochromator, fixed divergence slit ( $1/4^\circ 2\theta$ ), and the X'Celerator detector system as described by Vogt (2009).

Carbonate content was measured from the fine sediment fraction. Approximately 0.5 g of this fine material was powdered with a mortar and pestle and analyzed for carbonate content using a modified Müller and Gastner's (1971) "Karbonat-Bombe" technique. 0.2-0.5 g of material instead of 1 g, and 10 ml 20% 2.3 N HCl were used instead of 5 ml concentrated HCl. Resulting pressure was calibrated frequently with a reference curve generated using varying amounts of pure carbonate material to calculate percent carbonate of sample material.

Mass accumulation rate ( $MAR_{\text{Sil, Carb, or Arag}}$ ) was calculated to determine the amount of a specific sediment deposition by mass over time. Percent carbonate content was used with linear sedimentation rate (LSR) and bulk density ( $\rho_b$ ) to calculate carbonate MAR and by subtraction siliciclastic MAR (Eq. 1). Density data was published in Webster et al. (2011).

$$\text{Eq. 1} \quad MAR_{\text{Sil or Carb}} = (100 - \text{carbonate \%}) * \text{LSR} * \rho_b$$

Three lithoclastic packstone to grainstone samples were selected from a core interval (core 4 section 1 of Hole 58A, 9.1, 9.3, and 9.5 mbsf) thought to correspond to the Last Glacial Maximum (LGM) for petrographic examination. The thin-sections were analyzed for grain types, cementation, and diagenetic processes by counting 300 points under a LEICA petrographic

microscope (van der Plas and Tobi, 1965; Gischler et al., 2013). Relative amounts of carbonate minerals were measured by XRD as described by Milliman (1974, p. 21-27). Insoluble residue was determined by weighing sub-samples before and after dissolution in 10% HCl.

## RESULTS

### *Sedimentology*

**Visual Description.**---The sediment composition in Hole 58A on the upper fore reef slopes off the Central Great Barrier Reef exhibit parts of three fining upward successions. Seven lithostratigraphic units are distinguished based on color and grain size in Hole 58A, with Unit 1 located at the top and Unit 7 at the base (Fig. 2; Webster et al. 2011). Throughout the hole, neritic and pelagic skeletal carbonate grains vary in dominance in the coarse sediment fraction (>63  $\mu\text{m}$ ). Coral fragments commonly are not large enough to be visually observed and are only a very minor constituent. These lithologic units generally fit with the more detailed compositional analysis of Hole 58A sediments. In general, Units 7, 4, and 1 (Webster et al. 2011) include high proportions of the fine fraction, high carbonate content, high light reflectance, and low magnetic susceptibility (Fig. 3).

Thin-sections of three lithoclasts within Units 2 and 3 (located at 9.25, 9.44 and 9.585 mbsf) consist of lithified fine to medium mostly carbonate sand, commonly encrusted by non-geniculate coralline algae and serpulids (Table 1). The lithoclasts selected from Unit 2 within Hole 58A consist of mollusk-foraminifera-bryozoan packstone to grainstone with marine high-Mg-calcite cement (peloidal cement predominating) and display no evidence of meteoric diagenesis. Bioclast specific constituents and amounts vary (Table 1).

**Grain Size.** The fine fraction ( $<63\ \mu\text{m}$ ) of Hole 58A shows a wide range of roughly cyclic variations, from 0% to 94% (Fig. 3). Three intervals of 50% to 94% fines are separated by two coarse intervals, the lower of which occurs from 32.5 – 28.8 mbsf, though much of the interval is not recovered between 30.5 and 42.4 mbsf. The top of the upper coarse interval is defined at 7.1 mbsf, but its lower boundary is poorly defined due to non-recovery between 14.6 and 9.9 mbsf (Fig. 2, Fig. 3).

**Carbonate Content.** Carbonate content values from the Hole 58A fine fraction ( $<63\ \mu\text{m}$ ) range from between 30% and 85%, with two specific intervals of lower than 60% carbonate (Fig. 3). The lower interval is between 32.5 – 28.8 mbsf, while the upper low carbonate interval falls between 18.5 – 6.0 mbsf. In these intervals with carbonate content lower than 60%, the coarse fraction grains are dominated by carbonate particles: larger benthic foraminifera, mollusk and gastropod skeletal fragments, echinoid fragments, and planktic foraminifera with low amounts of frosted quartz grains. The bulk carbonate content of the three grainstone and packstone lithoclasts from the upper low carbonate content interval ranges from 90 – 98%, based on mass of insoluble residue (Table 1). Throughout the core, the coarse fraction dominantly consists of planktic and benthic foraminifers along with varying amounts of whole and fragmented pteropods, gastropods, pelecypods, bryozoans, echinoids, green algae, and peloids. Coarse grains ( $>63\ \mu\text{m}$ ) are comprised almost completely of carbonate grains, thus downhole variations away from pure carbonate in the carbonate content is a reflection of fine fraction sediment composition. In the high carbonate content intervals, the overall values increase upwards whereas fine grained material decreases.

### *Physical Properties*

**Color Reflectance.** Reflectance data values varies from 34 to 62 L\* with low and high reflectance arbitrarily separated at 48 L\*(Fig. 3). Sediment color, measured as light reflectance, is associated with sediment composition - high reflectance values corresponding with light colored carbonate intervals and low values with dark colored terrigenous siliciclastic material. The overall shape matches well with the shape of the carbonate content curve. Two intervals less than 48 L\* at depths of 32.6 – 26.8 mbsf and 18.6 – 5.9 mbsf align well with the two low carbonate content intervals. In addition to these two intervals, the overall variations of light reflectance match well with the shape of carbonate content variation. Correlation between carbonate content and light reflectance yields a statistically significant ( $P\text{-value} = 5.28 \times 10^{-16}$ )  $R^2$  value of 0.73.

**Magnetic Susceptibility.** Magnetic susceptibility (MS) values from U-channel data (Herrero-Bervera and Jovane 2013) range from  $-0.22 \times 10^{-5}$  to  $52.74 \times 10^{-5}$  SI and most of the values do not exceed  $\sim 10 \times 10^{-5}$  SI (Fig. 3). Three low MS intervals ( $< 10 \times 10^{-5}$  SI), correspond with intervals of high light reflectance and high carbonate content, and are separated by two intervals of MS higher than  $10 \times 10^{-5}$  SI located between 32.6 – 27.0 mbsf and 9.6 – 6.9 mbsf.

**Density.**---MSCL (multi-sensor core logger) Bulk Density increases with depth downhole from 1.60 to 2.00 g/cm<sup>3</sup> reaching 2.32 g/cm<sup>3</sup> within the hard ground  $\sim 10$  mbsf. Discrete dry bulk density (DBD) measurements follow the same trend, though consistently lower than MSCL values, ranging from 1.57 to 1.86 g/cm<sup>3</sup> with a peak of 2.62 g/cm<sup>3</sup> at the hard ground interval (Webster et al. 2011). It is important to note that there is no density anomaly found within TII and MIS-5 (the time of focus). The core liner was not full within core 2 and a portion of core 3 resulting in the underestimation of WBD by the MSCL. DBD measurements were not affected by the core liner issue.

### *Mineralogy*

The most abundant minerals from discrete bulk sediment samples analyzed by XRD are aragonite, low-Mg-calcite, high-Mg-calcite, quartz, feldspar, and clay minerals (Figs. 4 and 5). Throughout Hole 58A, aragonite and quartz are the main contributors to the carbonate siliciclastic sediments, respectively. Strontium (Sr) and silica (Si) variations in Hole 58A, obtained by XRF core scanning and used as proxies for aragonite and siliciclastics respectively, yield high resolution records of aragonite and siliciclastic sedimentation (Fig. 4).

**X-Ray Diffraction.** Analyzed samples show reciprocity between carbonate and siliciclastic minerals. With a few exceptions, carbonate minerals make up the majority of the bulk composition within Hole 58A, ranging from 28% to 76%, whereas siliciclastics range the inverse from 24% to 72% of bulk sediments. XRD of the bioclasts show average mineral compositions of 39% aragonite, 51.5% high-Mg-calcite, and 9.5% low-Mg-calcite.

In the bulk sediment, aragonite ranges from 9% to 41%, high-Mg-calcite from 0% to 33%, and low-Mg-calcite from 5% to 24% (Fig. 4). Three high aragonite content intervals (>25%), peaks occurring at 34 mbsf (40%), 23.8 mbsf (41%), and at the sea floor (37%), are separated by two intervals of low aragonite between 31-27 mbsf and 19-8 mbsf (Fig. 4). With only a few aragonite constituents (mostly pteropod fragments) identified within the coarse fraction, fine aragonite is expected to be found dominantly within the fine grained carbonate at Hole 58A. High-Mg-calcite in bulk sediments rarely exceeds 15%; the two exceptions are from 31-29 mbsf with a peak of 24% and 9.5-9.3 mbsf peaking at 33% which correspond with intervals of coarse sediment (Fig. 4). XRD from the three grainstone to packstone lithoclasts contained ~50% high-Mg-calcite related to skeletal grains and cement. In general, lower amounts of low-Mg-calcite compared to aragonite, exhibit similar cyclicity with lower

amplitudes. Intervals characterized by low proportions of low-Mg-calcite (<12%) occur from 31-26.2 mbsf and 16.5-3.2 mbsf; these low-Mg-calcite intervals extend to slightly shallower depths than aragonite. Variation and peak intensity is uniformly low within the three high low-Mg-calcite intervals (>12%), with values rarely exceeding 22% (Fig. 4).

Siliciclastic minerals (quartz, feldspars, and clays) are present in varying amounts and generally follow similar trends with some notable exceptions. The bulk abundance of quartz ranges from 8% to 40%, feldspars from 0% to 22%, and clay minerals from 5% to 24% (Fig. 5). High bulk quartz quantities (>20%) are present within two intervals from 31.0-25.6 mbsf (peaking at 40%) and 16.9-3.7 mbsf (peaking at 37%) (Fig. 5). These intervals of high quartz generally conform to the boundaries of low carbonate content and high magnetic susceptibility. Bulk feldspar comprises less than 10%, with two thin intervals where bulk feldspar range between 10 and 20% coinciding with highest quartz intervals. The amount of clay minerals is consistently between 5-20%, with a major high interval between 21.0-26.5 mbsf where clay minerals are all between 13-23%.

**X-Ray Fluorescence.**---XRF scanning of Hole 58A, for strontium (Sr) and silica (Si), yield elemental data at 1 cm intervals as useful proxies for shelf derived neritic carbonate (Figs. 4 and 6) and terrigenous siliciclastics (Fig. 5). Other elements such as potassium and titanium are also useful for determining terrigenous input; however, their trends are very similar to Si and are not considered in this study. Sr counts range from 2,000 to 11,000 with two intervals lower than 7,000 at the same depths as low carbonate content intervals, at 32.5 – 28.8 mbsf and at 18.5 – 6.0 mbsf. The substitution of Sr for Ca within the orthorhombic lattice of neritic aragonite (coral and green algae) is well established (Milliman 1974; Boardman and Neumann 1984; Dunbar and Dickens 2003a) and, as is the case at Hole 58A, plotted Sr counts and discrete bulk



percent aragonite displays a statistically significant fit (Fig. 6a) with  $R^2 = 0.85$  (P-value =  $3.69 \times 10^{-8}$ ; Fig. 6b), establishing Sr as a reliable proxy for neritic aragonite.

### *Sediment Chronology*

Due to incomplete sediment recovery at Hole 58A, the planktic  $\delta^{18}\text{O}$  isotope record of Hole 58A has been compared to the complete record at nearby MD-49 (Jorjy et al. 2010) to correlate between the two records and individual marine isotope stages (MIS) (Fig. 7). The remarkably similar shape and amplitude of these records strengthen the interpretation of glacial-interglacial MIS (well observed by the overlaying of the two records, Fig. 8). Based on the MIS interpretation of MD-49, the base of the upper recovered interval at Hole 58A is interpreted to include part Termination I and MIS-1 (Fig. 7). The Lisiecki and Raymo (2005) stacked benthic isotope record provided ages to marine isotope stage events identified within the Hole 58A and MD-49 records (Table 2). The base of Hole 58A contains a portion of MIS-7, the well-developed deglacial transition from the end of MIS-6 to MIS-5e, and most of MIS-5. Much of the MIS-6, 4, 3, and 2 glacial intervals are missing due to problems with core recovery leading to glacial age uncertainty. However, Hole 58A is well anchored during the Holocene by  $^{14}\text{C}$  age dating and within TII by biostratigraphy (Fig. 7). Three  $^{14}\text{C}$  ages of  $693 \pm 4$ ,  $4460 \pm 58$ , and  $6560 \pm 90$  yr-bp fit well within the second half of MIS-1 or the Holocene. The disappearance of *G. ruber* (pink-pigmented) during the MIS-6/5e transition 125 ka (Thompson 1979) anchors Termination II in Holes 58A, 820A, and MD-49, whereas this disappearance is more transitional, but still useful to identify Termination II in Hole 819A, (Fig. 7).

The same method was applied to develop a new depth-age model within the upper 55 m at Holes 820A (Peerdeman and Davies 1993) and upper 30 m at Hole 819A (Davies et al. 1991; Alexander et al. 1993; Fig. 7). Both Holes 820A (planktic *G. ruber*) and 819A (benthic

*Cibicidoides spp.*) include curves very similar in shape to Hole 58A and MD-49 (Fig. 7). Interpretations of  $\delta^{18}\text{O}$  at Hole 820A by Peerdeman and Davies (1993) do not account for the fact that, between 8-21 mbsf,  $\delta^{18}\text{O}$  values (between 1.5-2.0 ‰) are more consistent with MIS-5d to 5a than with MIS-3 (between 1.0-1.5 ‰) as at Hole 58A and MD-49. Additionally, based upon four radiocarbon dates between 7-7.5 mbsf available in Dunbar et al. (2000) (the youngest at 14.8 ka, and the three oldest 31, 41, and 43 ka (essentially carbon dead)), as at Hole 58A, most of MIS 4-3 and 2 are missing, and as such stable isotope chronology is the best method for determining sediment age between 8 and 30 mbsf at Hole 820A. MIS-5d to 5a is potentially difficult to discern as isotope variations are not as dramatic as those during TII. The validation of these depth-age models are clear once the four  $\delta^{18}\text{O}$  records for Holes 58A, 820A, 819A, and MD-49 are plotted in time beside one another and compared to the stacked LR04  $\delta^{18}\text{O}$  record (Fig. 8). Moreover, once plotted on top of another, the  $\delta^{18}\text{O}$  records on time for Hole 58A and MD-49 fit well (Fig. 8). By establishing a depth-age model for Hole 58A, physical parameters and sediment composition can be plotted with respect to time instead of core depth and lithologic units (Fig. 9).

### *Sediments in Time*

The fine fraction roughly matches glacial-interglacial stages, highest values of fines correspond with interglacial times (MIS-5e and Holocene) and the lowest values occur during glacial times (MIS-6 and MIS-2; Fig. 9). High fine fraction values are also evident during late MIS-7 and early MIS-6. Contrarily, the carbonate content of the fine fraction is not in phase with glacial-interglacial cycles.

Low carbonate content (36%) occurs at the beginning of MIS-5e and increases to a maximum (84%) at the end of MIS-5e. A similar trend is observed during MIS-1 with carbonate

content increasing from a minimum values (45%) to maximum (78%) at present. During the remainder of MIS-5, carbonate content remains high until the beginning of MIS-5b where it decreases to a local minimum at the beginning of MIS-5a. Fine carbonate content values increase from an average of 65% at the end of MIS-7 to above 80% in early MIS-6, surprisingly, with values as high as late MIS-5e. Light reflectance and magnetic susceptibility, well established proxies for carbonate content, mimic the trends observed in the carbonate content (Fig.9). As most of the sediments are fine-grained and nearly all of the coarse grains are identified as low and high-Mg-calcite producers, Sr-rich (neritic) aragonite must be the dominant mineralogy through most of Hole 58A.

Only bulk carbonate was measured at Holes 820A and 819A; the carbonate content trends are remarkably similar to the ones observed in Hole 58A (Fig. 10). The dramatic carbonate increase within MIS-5e is observed in the three Holes and the carbonate values remain high throughout MIS-5d-b and drop to a minimum during early MIS-5a and increase to a maximum at the end of 5a. Not only are carbonate content trends strikingly similar at Holes 58A, 820A, and 819A, but the relative magnitude of carbonate content fluctuations are very similar and display many of the same smaller scale variations (Fig. 10). This MIS-5 trend, particularly well observed at Holes 58A and 819A (Fig. 10), contrasts with the carbonate variation roughly in phase with glacial-interglacial cycles observed in MD-49. The MIS-5e is well characterized by carbonate content values ranging between 80 and 90%, whereas the values at the end of MIS-6 and the beginning of MIS-5d barely reach 10%. Carbonate content reaches the lowest values during the second half of MIS-5, in particular at the beginning of MIS-5d and -5b, out of phase with the trend observed in Holes 58A, 819A, and 820A.

#### *Siliciclastic Mass Accumulation Rates*

MAR<sub>Sil</sub> (units of  $\text{g}\cdot\text{cm}^{-2}\cdot\text{kyr}^{-1}$  not repeated in section for brevity) at Hole 58A (Fig. 11) illustrate how terrigenous-based sediment flux to the upper slope is variable in time, as a result to climate change and sea level fluctuations. During rising sea level at Termination II, MIS-6 to MIS-5e, MAR<sub>Sil</sub> transitioned from low  $\sim 8$  to  $\sim 60$  between 133 ka and 130 ka (Fig. 11). At the MIS-6/5e boundary (130 ka), MAR<sub>Sil</sub> dropped suddenly to  $\sim 10$ -12 until the MIS-5e interglacial peak (123 ka). During the subsequent sea-level fall, MAR<sub>Sil</sub> increase to  $\sim 27$ , and then decline to  $\sim 10$  at 115 ka. MAR<sub>Sil</sub> remain low throughout MIS-5d and 5c, but rapidly increase to over 50 within MIS-5b (87.5 ka) peaking at nearly 80 in early MIS-5a (83 ka) and then decline to  $\sim 60$  at the end of recovery.

At Hole 820A, MAR<sub>Sil</sub> is very similar to Hole 58A. MAR<sub>Sil</sub> rises from  $\sim 5$  to  $\sim 28$  by 140 ka and decreases gradually to  $\sim 20$  at 123 ka, followed by a significant increase to  $\sim 50$  at 123 ka followed by a slow decline until MIS-5b (Fig. 11). MD-49 begins in a similar manner with increasing MAR<sub>Sil</sub> from  $\sim 10$  to 20 at 140 ka. However, at 133 ka MAR<sub>Sil</sub> declines to  $\sim 5$  where it remains until 115 ka when MAR<sub>Sil</sub> increases gradually to  $\sim 25$ . At 96 ka, MAR<sub>Sil</sub> increases significantly to nearly 60 before slowly falling off towards the peak of MIS-5a (Fig. 11).

#### ***Aragonite/Carbonate Mass Accumulation Rates***

The fine-grained neritic sediment flux to the upper slope is described by the variations of MAR<sub>Arag</sub> at Hole 58A compared to sea level fluctuations (Figs. 11 and 12; Rohling et al. 2008). During Termination II, MAR<sub>Arag</sub> values reach  $\sim 20 \text{ g}\cdot\text{cm}^{-2}\cdot\text{kyr}^{-1}$  (units not repeated in section for brevity) locally from 133 to 131 ka and then decline to minimum values of  $\sim 1$ -3 during the peak sea level of MIS-5e (130 – 123 ka) (Fig. 12). The MAR<sub>Arag</sub> increase to 21 during the second half of MIS-5e and peak at  $\sim 25$  during the transition from MIS-5e to MIS-5d, when sea level drops by as much as 55 m. During the late MIS-5d to early MIS-5b interval, MAR<sub>Arag</sub> drop to  $\sim 13$  and

reach a minimum of  $\sim 8$  during MIS-5b when sea level fell from  $\sim 40$  m to  $\sim 70$  m, largely exposing the shelf, respectively.  $MAR_{Arag}$  increase to a maximum of  $\sim 30$  during the transition from MIS-5b to MIS-5a when sea level rose back to  $\sim 30$  m.

Aragonite content data are not available at Hole 820A, thus  $MAR_{Arag}$  cannot be calculated.  $MAR_{Carb}$  was calculated at Hole 820A and shows striking similarities with  $MAR_{Carb}$  at Hole 58A (Fig. 11). The  $MAR_{Arag}$  are very similar in shape to  $MAR_{Carb}$  at Hole 58A, thus we use  $MAR_{Carb}$  as a general tentative trend for  $MAR_{Arag}$  at Hole 820A. In general,  $MAR_{Carb}$  at Hole 820A are higher than at Hole 58A. During TII,  $MAR_{Carb}$  rise to  $\sim 30$  by early MIS-5e, then  $MAR_{Carb}$  become low (10-15) before increasing to over 70 in the second half of MIS-5e, followed by a consistently lower interval until 87 ka. During much of MIS-5a,  $MAR_{Carb}$  at Hole 820A increase but less pronounced, compared with Hole 58A. Although MAR is not available for Hole 819A, the similarity of its carbonate content with Holes 58A and 820A (Fig. 10) suggests that MAR at this location will exhibit the same patterns as found at Holes 58A and 820A (Fig. 11).

## DISCUSSION

The results at Hole 58A, as well as Holes 820A and 819A, are focused on the interval (150 – 75 ka) spanning the penultimate glacial (MIS-6), Termination II (transition from MIS-6 to MIS-5e), and the last interglacial (MIS-5). These successions display a distinctly cyclical accumulation of siliciclastic and carbonate sediments that largely are the result of interactions among sea level, shelf bathymetry, and variations in monsoon intensity.

### *GBR Margin Sedimentation over the Last 30 kyr*

Sedimentation along the GBR margin has been shown to be increasingly dynamic with increasing proximity to the reef. According to Dunbar et al. (2000) and Dunbar and Dickens (2003b) LSR ( $\text{cm ky}^{-1}$ ) and MAR, ( $\text{Mt yr}^{-1}$ ) varied according to sea level and distance from the GBR platform over an area of  $\sim 32000 \text{ km}^2$ . During the LGM, when sea level was generally below the GBR shelf break in the study area ( $-70$  to  $-80 \text{ m}$ ) from  $14.7 - 31 \text{ ka}$ , MAR were consistently low from shelf to basin ( $0.27$  and  $0.38 \text{ Mt yr}^{-1}$ ) and dominated by carbonate sediments. During transgression when the shelf was flooded ( $6.5 - 14.7 \text{ ka}$ ), sedimentation increased dramatically along the central GBR upper slope ( $2.1 \text{ Mt yr}^{-1}$ ) but was only slightly more elevated within the basin ( $0.5 \text{ Mt yr}^{-1}$ ). Siliciclastic and carbonate sedimentation were nearly equal in rate on the slope ( $1.0$  and  $1.1 \text{ Mt yr}^{-1}$  respectively), although carbonates dominated basin sedimentation ( $0.4$  to  $0.1 \text{ Mt yr}^{-1}$ ). Sedimentation rates during the subsequent highstand ( $0 - 6.5 \text{ ka}$ ) along the slope remained high with respect to carbonates ( $1.4 \text{ Mt yr}^{-1}$ ) with a marked decline in siliciclastic sedimentation rates ( $0.3 \text{ Mt yr}^{-1}$ ). Basin sedimentation rates continued to remain low during the highstand. Presently, outer shelf, slope, and basin (Queensland Trough) sediments are dominated ( $> 70 - 80\%$ ) by carbonate grains with the exception of a siliciclastic tongue ( $40 - 60\%$  siliciclastics) extending from the Ribbon Reef portion of the GBR to the south into the Queensland Trough (Dunbar and Dickens 2003a; Francis et al. 2007). From these studies (Dunbar et al. 2000; Dunbar and Dickens 2003b; Page et al. 2003; Page and Dickens 2005), it is clear that the sedimentary response of the GBR to sea level is best recorded on the slope where sediment variation is greatest. Dunbar and Dickens (2003a) have also shown that the amount of aragonite and high-Mg-calcite (generally neritic carbonate sourced) within the upper slope sediments is much higher at positions proximal to the reef than positions within the basin. Most of the carbonate variation over time likely is tied to

increased neritic carbonate production on the GBR shelf, when the shelf is flooded and sediment is exported to the upper slope. In contrast, the carbonate MAR in the basin is mostly sourced from a consistent flux of planktic and *in situ* benthic carbonate production.

Data from the northern GBR suggest a MAR distribution over the time since the last LGM similar to the central GBR. Carson et al. (2008) and Jorjy et al. (2010) have shown that during the lowstand conditions leading up to the TI transition, carbonate and siliciclastic sedimentation rates were extremely low, followed by substantial increases in carbonate and siliciclastic accumulation on the northern GBR upper slope when the shelf was flooded at ~11 ka (as seen at many cores in the area MD-49, MD-34, MV74, MV-07/06, MV-17, and MV-13; Francis 2007; Carson et al. 2008; Jorjy et al. 2010). Neritic carbonate highstand shedding commonly is reported during the Holocene along the GBR margin (Dunbar and Dickens 2003a), and consistent with the recent concepts of the ‘re-flooding window’ (Jorjy et al. 2010) and ‘production window’ (Maldives Inner Sea – Paul et al. 2012) that occur when carbonate platforms are flooded and production is initiated. Though core recovery in the upper part of Hole 58A, representing the last 20 ky, is not continuous and MSCL density errors within the upper 8 m make accurate MAR calculation difficult, recovered sediments are consistent with published observations in the GBR of increased siliciclastic sedimentation during TI, especially as seen at Hole 820A (Figs. 9 and 10). There is a pronounced increase in fine siliciclastics at (Figs. 5 and 9) that is consistent with an increase in fine siliciclastics at Hole 820A from 6-7 mbsf (Peerdeman and Davies 1993). At Hole 820A, this increase in fine siliciclastics is related to the increased  $MAR_{Sil}$  that occurred during TI, and therefore, we infer that a similar high  $MAR_{Sil}$  during also occurred at Hole 58A during T1.

#### *Siliciclastic Sediment Flux to the Upper Slope from 150 ka to 75 ka*

The pulse of siliciclastic sediment to the upper slope during the last sea level rise could be explained either by the reworking of siliciclastic material trapped on the exposed shelf during times of relatively low sea level or the increase in the Australian monsoon during deglacial time resulting in increased weathering and transport of terrigenous material to the slope through the water column (Dunbar et al., 2000; Dunbar and Dickens, 2003a). At Hole 58A, similar processes might have caused the large siliciclastic pulse that occurred during Termination II and interglacial MIS-5.

During sea level rise from MIS-6 to MIS-5e, the shelf is re-flooded and siliciclastic sediments stored on the shelf during MIS-6 would have been reworked by transgressive ravinement and transported to the upper slope (Fig. 13b) resulting in the large increase in  $MAR_{Sil}$  (Fig. 11) that has been described in sequence stratigraphic terms as healing phase deposition (Posamentier and Allen 1999). Dunbar et al. (2000) favored reworking as they found sediment fluxes to be too great for precipitation alone coupled with a large amount of mangrove pollen (Grindrod et al. 1999; Moss and Kershaw 2007), suggested the reworking of marine sediments. However, as sea level reached maximum during MIS-5e, reworking would cease, and siliciclastic material would be restricted to the coastline (Fig. 13c). High carbonate and siliciclastic sedimentation rates during TII and during transgression into MIS-5a also occurred in the southern GBR (Page and Dickens 2005). Based on Lake Eyre shorelines (Magee et al. 2004), maximum monsoon intensity over the last 150 ky occurred during MIS-5e and would have dramatically increased precipitation and potentially sediment transport to the shelf. Pollen data from Lynch's Crater, northeastern Queensland, confirms that precipitation was high during MIS-5, low during MIS-4 to 2, and high again during TI (Kershaw 1986). As for late Holocene GBR system (Dunbar and Dickens, 2003a; Francis et al., 2007), the relatively narrow GBR shelf



would have allowed part of the fine siliciclastic material to bypass and accumulate on the upper slope during late MIS-5e. The increased sediment supply to the slope is not evident in the upper slope of the northern GBR, probably as the GoP shelf is large enough (> 150 km wide) to capture increased siliciclastic flux within an inner shelf mud clinoform, as observed in the present GoP shelf (Slingerland et al. 2008; Tcherepanov et al. 2010).

Interestingly, the maximum  $MAR_{Sil}$  values along the central GBR occur as a large pulse during late interglacial MIS-5a (Fig. 11). From MIS-5d to MIS-5b, sea level was between 40 and 50 m lower than today. This extended period of low sea level exposed most of the inner shelf during MIS-5b and allowed siliciclastic sediments to accumulate on the middle shelf, much like the early Holocene, when large amounts of siliciclastics accumulated on the middle shelf within a coastal setting ~10 ka (Heap et al. 2002). As sea level rose during MIS-5a to -20 m, levels not achieved since MIS-5e (Rohling et al. 2008; Dorale et al. 2010), siliciclastic sediment within the middle shelf was reworked once again, resulting in transgressive shedding to the central GBR upper slope. Dunbar et al. (2000) made note of this increase of siliciclastic sediments during MIS-5b to 5a, but did not provide a compelling explanation. This interpretation contrasts with data from the northern GBR, where major siliciclastic pulses are associated with periods of lower sea level, especially MIS-5b, that lead to the reworking of the inner GoP shelf prograding clinoform (Jorry et al. 2010).

#### *Neritic Carbonate Shedding to the Upper Slope*

From the LGM to Holocene interglacial, the  $MAR_{Carb}$  follow closely the highstand shedding model, in which the re-flooding of a shelf or platform and the establishment of optimum sea level conditions allows corallgal reefs to form on submerged topographic highs leading to increased production of neritic carbonate (Webster et al. 2011), which is then shed to

the nearby upper slope (Schlager et al. 1994). Highstand shedding, initiated at  $\sim 11.5$  ka, is clearly observed during Termination I and II at MD-49 in the GoP (Jorjy et al. 2010), in Ashmore (Francis 2007) and Pandora Troughs (Jorjy et al. 2008) during Termination I. It would be expected that the optimal growth conditions created during maximum sea level of MIS-5e would also result in prolific corallgal reef establishment and subsequent neritic carbonate shedding to the upper slope. However, this situation is not the case for the central GBR, where neritic carbonate shedding during MIS-5 is out of phase with the highstand shedding model.

During Termination II sea-level rise from MIS-6 to MIS-5e, the GBR shelf was re-flooded and incipient reefs formed, resulting, as expected, in the increase of  $MAR_{Arag, Carb}$  at Hole 58A (Figs. 12 and 13b). However, when maximum sea level was reached during MIS-5e,  $MAR_{Arag, Carb}$  values were at their lowest level (Figs. 12 and 13c). This decline in neritic carbonate shed to the central GBR upper slope is attributed to the drowning of the GBR on the shelf edge during early MIS-5e (Fig. 13c). Based on detailed and systematic data (Montaggioni 2005) and models (Kim et al. 2012), reefs can drown based on how fast sea level rises during the initial flooding without additional environmental stressors. However, the drowning of reefs is paradoxical as rates of sea-level rise are generally insufficient alone to drown carbonate platforms (Schlager, 1981), and that environmental factors such as increased turbidity and nutrients and decreased salinity can lead to reef growth rates falling below their accretion potential during times of particularly rapid sea level rise (Kiessling 2009). During TII, sea level may have risen as rapidly as 6-9 mm/yr, which is 2-3 time higher than present yet half as much as Meltwater Pulse – 1A (Kopp et al. 2009). For the central GBR, we propose a combined effect of very high sea level rise conditions together with diminished coral accretion due to environmental stressing factors to explain why  $MAR_{Carb, Arag}$  lags the highstand shedding model

prediction for MIS-5e by ~10-15 kyr (Fig. 11, 12). The monsoons during MIS-5e (Kershaw 1986; Magee et al. 2004) led to increased runoff, which conceivably resulted in the increase of nutrient transport to the GBR (Kleinman et al. 2006). High  $MAR_{Sil}$  during TII (Fig. 11, 12) suggest that turbid water may have been a stressor of the fledgling reef hindering its ability to keep up with sea level rise that may have been as rapid as 6-9 mm/yr (Kopp et al. 2009; Kiessling 2009). Increased sedimentation from the Amazon River coupled with rapid sea level rise is suspected to have caused a similar reef demise during over time during the Miocene in the Foz do Amazonas Basin (Gorini et al. 2014).

The five-fold increase in  $MAR_{Arag, Carb}$  at Holes 58A and 820A indicate reef recovery occurred in the end of MIS-5e when sea level began to fall and drowned GBR highs re-entered the optimal euphotic zone (Fig. 13d). Similar trend of nearly doubled  $MAR_{Arag}$  during MIS-5a to 5d over MIS-5e has been also recorded in the Maldives Inner Sea (Paul et al., 2012). This result in the central GBR is in contrast with the northern GBR, where  $MAR_{Carb}$  are highest during peak interglacial, MIS-5e, and decline at the same time that carbonate production is increasing in the central GBR (Fig. 11). The shallower bathymetry of the carbonate factory and clockwise currents on the GOP shelf that transport siliciclastic sediment and nutrients from GOP rivers away from the GBR to the northeast (Slingerland et al. 2008) may explain how MD-49, along the northern GBR within Ashmore Trough, displays high carbonate sedimentation rates during peak interglacial times consistent with classical carbonate highstand shedding, while carbonate sedimentation along the central GBR was not. The drop in sea level following peak interglacial MIS-5e would have exposed nearly all of the northern GBR shelf and Ashmore Reef (Jorjy et al. 2010), cutting off carbonate sediment supply to the northern GBR upper slope.

Highstand shedding has been a documented globally in the present in the Bahamas, Droxler and Schlager 1985; Boardman et al. 1986), Nicaragua Rise (Glaser and Droxler 1991), Maldives (Paul et al. 2012), Gulf of Papua and Caribbean (Jorjy et al. 2010). All of these cases have benefitted from well dated sediments in the context of sea level. In the geologic past sea level is less certain, yet highstand shedding is used to describe carbonate sedimentation as part of the reciprocal sedimentation model in many outcrops (Wilson 1967; Sarg 1988; Dolan 1989; Handford and Loucks 1993). Shanmugam and Moiola (1984) postulated that some Campanian-Maastrichtian calciturbidites occurred during the lowering sea level or even lowstand. Additionally, there is evidence for regressive carbonate shedding having occurred in the Late Cretaceous Alps of France (Jacquin, 1990), though this has since come into question (Schlager et al., 1994). This study of the modern GBR slope does not prove these interpretations as correct, it only provides a modern analog for the possibility of carbonates being shed off bank during the lowering of sea level or even lowstand.

A major increase in  $MAR_{Arag, Carb}$  within the central GBR, at Holes 58A and 820A, follows a period of slowly declining neritic carbonate shedding to the upper slope. This pulse of neritic carbonate to the upper slope occurs at the end of MIS-5b and within MIS-5a when sea level is thought to have increased to levels not attained since MIS-5e (Rohling et al. 2008; Dorale et al. 2010), resulting in carbonate shedding during a brief period of rising sea level during a time interval of general falling sea level (Fig. 13d).

## CONCLUSIONS

Upper slope sediments at Holes 58A, 820A/B, and 819A along the tropical mixed carbonate-siliciclastic central GBR margin, consist of two dominant sediment sources:

alternating to coeval terrigenous siliciclastics and neritic carbonates. The timing of this alternating accumulation has classically been described by the reciprocal sedimentation model and the highstand shedding concept, maximum accumulation of siliciclastic during lowstand and carbonates during highstand. Based on the results of this study the maximum accumulation rates of carbonates and siliciclastics are out-of-phase with the prediction of these models from the last 150 to 75 ka. The sequence of events occurred as follows:

During sea level rise, glacial-interglacial transition MIS-6/5e (Termination II), sedimentation rates increased significantly and were dominated by fine-grained siliciclastics as the result of either ravinement of terrigenous material previously trapped within alluvial plains during shelf exposure or by increased siliciclastic sediment supply due to the increase of monsoons following long periods of drought.

During peak sea level, interglacial MIS-5e, highstand shedding was minimal, whereas siliciclastic sediments dominated this period of lowest mass accumulation rates; these observations can be explained by a largely drowned central GBR and, therefore, unexpectedly low neritic production and export to the upper slope.

During the interval of falling sea level, last 2/3 of interglacial MIS-5 (MIS-5d/a), sea level fluctuated between 20 and 50 m below present sea level. This time interval is characterized by the highest accumulation rates on the upper slope. During MIS-5d to 5a, the central GBR reentered the photic zone, resulting in maximum neritic production and large export of reef derived fine sediment to the upper slopes. Moreover, the reworking of siliciclastics, temporarily stored on the inner and middle shelf, and their export to the upper slopes added to the large export of neritic carbonate.

Mixed margins are common both in the past and in the present; however, many of these systems have been studied without the constraint of well-established sea level curves. These results provide a case study for sea level related off-shelf sediment transport along a mixed margin that is in opposition to aspects of both the reciprocal sedimentation model and carbonate highstand shedding. Some ancient examples of carbonate shedding are believed to have occurred not at maximum sea level but as sea level lowered, this study validates this possibility. Carbonate off-bank transport occurs not necessarily during maximum highstand but when the bank top is flooded to a depth within the photic zone. These exceptions to the conceptual rules suggest that sedimentation of many ancient and modern mixed systems may be more complicated than previously thought.

## ACKNOWLEDGEMENTS

We are thankful for the Integrated Ocean Drilling Program for providing us with cores from Hole M0058A, and especially the Cruise 325 Scientific Party and Officers and Crew of the Great Ship Maya. We would like to thank Christoph Vogt for his work obtaining the XRD measurements from Hole. We would also like to thank Kazuyo Tachikawa for allowing the use of strontium for core scans at MD-49. Additionally, we would also like to thank Gerald R. Dickens for his discussions and insights about sedimentation on the central GBR slopes. We would also like to thank our reviewers: John Reijmer, Gregor Eberli, Gavin Dunbar, and editor: Gene Rankey for their thoughtful comments and suggestions.

This research was partially funded by IODP through a grant from the USSSP program from the Consortium for Ocean Leadership to Droxler and ARCD Grant (DP1094001) to Webster. TOTAL (Cecile Pabian-Goyheneche, Patrick Sorriaux, and Aurelien Virgone) provided

the major financial support through a grant to Rice University (Droxler), in addition to a Mills Bennett Fellowship at Rice University for Harper's PhD research.

## REFERENCES

- Alexander, I., Kroon, D., and Thompson, R., 1993, Late Quaternary paleoenvironmental change on the northeast Australian margin as evidenced in oxygen isotope stratigraphy, mineral magnetism, and sedimentology: *Proceedings of the Ocean Drilling Program, Scientific Results*, v. 133, p. 130-161.
- Andresen, N., Reijmer, J.J.G., and Droxler, A.W., 2003, Timing and distribution of calciturbidites around a deeply submerged carbonate platform in a seismically active setting (Pedro Bank, Northern Nicaragua Rise, Caribbean Sea): *International Journal of Earth Science*, v. 92, p. 573-592.
- Beaman, R.J., 2010, Project 3DGBR: a high-resolution depth model for the Great Barrier Reef and Coral Sea: Marine and Tropical Sciences Research Facility Project 2.5i, The Final Report, MTSRF, Cairns, Australia, p. 13 plus Appendix 1.
- Betzler, C., Pfeiffer, M., and Saxena, S., 2000, Carbonate shedding and sedimentary cyclicities of a distally steepened carbonate ramp (Miocene, Great Bahama Bank): *International Journal of Earth Science*, v. 89, p. 140-153.
- Boardman, M.R. and Neumann, A.C., 1984, Sources of periplatform carbonates: northwest Providence Channel, Bahamas: *Journal of Sedimentary Petrology*, v. 54, no. 4, p. 1110-1123.
- Boardman, M.R., Neumann, A.C., Baker, P.A., Dulin, L.A., Kenter, R.J., Hunter, G.E., and Kiefer, K.B., Banktop responses to Quaternary fluctuations in sea level recorded in periplatform sediments: *Geology*, v. 14, p. 28-31.
- Bostock, H.C., Opdyke, B.N., Gaga, M.K., and Fifield, L.K., 2009, Late Quaternary siliciclastic/carbonate sedimentation model for the Capricorn Channel, southern Great Barrier Reef province, Australia: *Marine Geology*, v. 257, p. 107-123.
- Carson, B.E., Francis, J.M., Leckie, R.M., Droxler, A.W., Dickens, G.R., Jorjy, S.J., Bentley, S.J., Peterson, L.C., and Opdyke, B.N., 2008, Benthic foraminiferal response to sea level change in the mixed siliciclastic-carbonate system of southern Ashmore Trough (Gulf of Papua); *Journal of Geophysical Research*, v. 113, F01S20, 20 p.
- Daniell, J.J., 2008, Development of a bathymetric grid for the Gulf of Papua and adjacent areas: a note describing its development: *Journal of Geophysical Research*, v. 113, F01S15., 15p.

- Davies, P.J., McKenzie, J.A., Palmer-Julson, A., et al., 1991, Site 819: Proceedings of the Ocean Drilling Program, Scientific Results, v. 133, p. 451-508.
- Davies, P.J., Symonds, P.A., Feary, D.A., Pigram, C.J., 1989. The evolution of the carbonate platforms of Northeast Australia, *in* Crevello, P.D., Wilson, J.L., Sarg, J.F., and Read eds., Controls on Carbonate Platform and Basin Development: SEPM, Special Publication 44, p. 233-258.
- Dolan, J.F., 1989, Eustatic and tectonic controls on deposition of hybrid siliciclastic/carbonate basinal cycles: Discussion with examples: AAPG Bulletin, v. 73, p. 1233-1246.
- Dorale, J.A., Onac, B.P., Fomós, J.J., Ginés, J., Ginés, A., Tuccimei, P., and Peate, D.W., 2010, Sea-level highstand 81,000 years ago in Mallorca: Science, v. 327, p. 860-863.
- Droxler, A.W., Schlager, W., and Whallon, C.C., 1983, Quaternary aragonite cycles and oxygen-isotope record in Bahamian carbonate ooze: Geology, v. 11, p. 235-239.
- Droxler, A.W., and Schlager, W., 1985, Glacial versus interglacial sedimentation rates and turbidite frequency in the Bahamas: Geology, v. 13, p. 799-802.
- Droxler, A.W., Haddad, G.A., Kroon, D., Gartner, S., Wei, W., and McNeill, D., 1993, 17. Late Pliocene (2.9 Ma) partial recovery of shallow carbonate banks on the Queensland Plateau: signal of bank-top reentry into the photic zone during a lowering in sea level, *in* McKenzie, J.A., Davies, P.J., Palmer-Julson, A., et al., 1993: Proceedings of the Ocean Drilling Program, Scientific Results, v. 133, p. 235-254.
- Dunbar, G.B., Dickens, G.R., and Carter, R.M., 2000, Sediment flux across the Great Barrier Reef Shelf to the Queensland Trough over the last 300 ky: Sedimentary Geology, v. 133, p. 49-92.
- Dunbar, G.B., and Dickens, G.R., 2003a, Late Quaternary shedding of shallow-marine carbonate along a tropical mixed siliciclastic-carbonate shelf: Great Barrier Reef, Australia: Sedimentology, v. 50, p. 1061-1077.
- Dunbar, G.B., and Dickens, G.R., 2003b, Massive siliciclastic discharge to slopes of the Great Barrier Reef Platform during sea-level transgression: constraints from sediment cores between 15°S and 16°S latitude and possible explanations: Sedimentary Geology, v. 162, p. 141-158.
- Esker, D., Eberli, G.P., and McNeill, D., 1998, The structural and sedimentological controls on the reoccupation of Quaternary incised valley, Belize Southern Lagoon: AAPG Bulletin, v. 82, p. 2075-2109.
- Ferro, C.E., Droxler, A.W., Anderson, J.B., and Mucciarone, D.A., 1999, Late Quaternary shift



of mixed siliciclastic-carbonate environments induced by glacial eustatic sea level in Belize, *in* Harris, P.M., Saller, A., and Simo, T., eds., *Advances in Carbonate Sequence Stratigraphy: Applications to Oil Reservoirs, Outcrops, and Models*: SEPM: Special Publication 63, p. 385-411.

Francis, J.M., 2007, Late Quaternary sediment dispersal and accumulation on slopes of the Great Barrier Reef mixed siliciclastic-carbonate depositional system, Gulf of Papua, Papua New Guinea and North Queensland Margin, Australia: Rice University, Dissertation, p. 304.

Francis, J.M., Dunbar, G.B., Dickens, G.R., Sutherland, I.A., and Droxler, A.W., 2007, Siliciclastic sediment across the north Queensland margin, (Australia): a Holocene perspective on reciprocal versus coeval deposition in tropical mixed siliciclastic-carbonate systems: *Journal of Sedimentary Research*, v. 77, p. 572-586.

Francis, J.M., Daniell, J.J., Droxler, A.W., Dickens, G.R., Bentley, S.J., Peterson, L.C., Opdyke, B.N., and Beaufort, L., 2008, Deep water geomorphology of the mixed siliciclastic-carbonate system, Gulf of Papua: *Journal of Geophysical Research*, v. 113, F01S16.

Gagan, M.K., Sandstrom, M.W., and Chivas, A.R., 1987, Restricted terrestrial carbon input to the continental shelf during Cyclone Winifred: implications for terrestrial runoff to the Great Barrier Reef Province: *Coral Reefs*, v. 6, p. 113-119.

Gischler, E., Ginsburg, R.N., Herrle, J.O. and Prasad, S., 2010, Mixed carbonates and siliciclastics in the Quaternary of southern Belize: Pleistocene turning points in reef development controlled by sea-level change: *Sedimentology*, v. 57, p. 1049-1068.

Gischler, E., Thomas, A.L., Droxler, A.W., Webster, J.M., Yokoyama, Y., and Schöne, B.R., 2013, Microfacies and diagenesis of older Pleistocene (pre-last glacial maximum) reef deposits, Great Barrier Reef, Australia (IODP Expedition 325): A quantitative approach: *Sedimentology*, v. 60, p. 1432-1466.

Gorini, C., Haq, B.U., Tadeu dos Reis, A., Silva, C.G., Cruz, A., Soares, E., and Grangeon, D., 2014, Late Neogene sequence stratigraphic evolution of the Foz do Amazonas Basin, Brazil: *Terra Nova*, v. 26, p. 179-185.

Grammer, G.M. and Ginsburg, R.N., 1992, Highstand versus lowstand deposition on carbonate platform margins: insight from Quaternary foreslopes in the Bahamas: *Marine Geology*, v. 103, p. 125-136.

Grindrod, J., Moss, P., and van der Kaars, 1999, Late Quaternary cycles of mangrove development and decline on the north Australian continental shelf: *Journal of Quaternary Science*, v. 14, p. 465-479.

Handford, C.R. and Loucks, R.G., 1993, Carbonate depositional sequences and systems tracts –

- 796 responses of carbonate platforms to relative sea-level changes, *in* Loucks, R.G., and Sarg,  
797 J.F., eds., Carbonate Sequence Stratigraphy; Recent Developments and Applications:  
798 AAPG Memoir 57, p. 3-41.  
799
- 800 Harris, P.T., Davies, P.J., and Marshall, J.F., 1990, Late Quaternary sedimentation on the Great  
801 Barrier Reef continental shelf and slope east of Townsville, Australia: Marine Geology,  
802 v. 94, p. 55-77.  
803
- 804 Heap, A.D., Dickens, G.R., Stewart, L.K., and Woolfe, K.J., 2002, Holocene storage of  
805 siliciclastic sediment around islands on the middle shelf of the Great Barrier Reef  
806 Platform, north-east Australia: Sedimentology, v. 49, p. 603-621.  
807
- 808 Herrero-Bervera, E., and Jovane, L., 2013, On the palaeomagnetic and rock magnetic constraints  
809 regarding the age of IODP 325 Hole M0058A: Geological Society, London, Special  
810 Publications, v. 373, p. 279-291.  
811
- 812 Jacquin, T., 1990, Systems tracts and depositional sequences in a carbonate setting: a study of  
813 continuous outcrops from platform to basin at the scale of seismic liens: Marine and  
814 Petroleum Geology, v. 8, p. 122-139.  
815
- 816 Jorry, S.J., Droxler, A.W., Mallerino, G., Dickens, G.R., Bentley, S.J., Beaufort, L., Peterson,  
817 L.C., and Opdyke, B.N., 2008, Bundled turbidite deposition in the central Pandora  
818 Trough (Gulf of Papua) since Last Glacial Maximum: linking sediment nature and  
819 accumulation to sea level fluctuations at millennial timescale: Journal of Geophysical  
820 Research, v. 113, F01S19.  
821
- 822 Jorry, S.J., Droxler, A.W., and Francis, M.F., 2010, Deepwater carbonate deposition in response  
823 to re-flooding of carbonate bank and atoll-tops at glacial terminations: Quaternary  
824 Science Reviews, v. 29, p. 2010-2026.  
825
- 826 Kershaw, A.P., 1986, Climatic change and Aboriginal burning in north-east Australia during the  
827 last two glacial/interglacial cycles: Nature, v. 322, p. 47-49.  
828
- 829 Kiessling, W., 2009, Geologic and biologic controls on the evolution of reefs: Annual Review of  
830 Ecology Evolution and Systematics, v. 40, p. 173-192.  
831
- 832 Kim, W., Fouke, B.W., Petter, A.L., Quinn, T.M., Kerans, C., and Taylor, F., 2012, Sea-level  
833 rise, depth-dependent carbonate sedimentation and the paradox of drowned platforms:  
834 Sedimentology, v. 59, p. 1677-1694.  
835
- 836 Kleinman, P.J.A., Srinivasan, M.S., Dell, C.J., Schmidt, J.P., Sharpley, A.N., and Bryant, R.B.,  
837 2006, Role of rainfall intensity and hydrology in nutrient transport via surface runoff:  
838 Journal of Environmental Quality, v. 35, p. 1248-1259.  
839
- 840 Kopp, R.E., Simons, F.J., Mitrovica, J.X., Maloof, A.C., and Oppenheimer, M., 2009,

- 841 Probabilistic assessment of sea level during the last interglacial stage: *Nature*, v. 462, p.  
842 863-867.
- 843
- 844 Lawrence, K.T., and Herbert, T.D., 2005, Late Quaternary sea-surface temperatures in the  
845 western Coral Sea: Implications for the growth of the Australian Great Barrier Reef:  
846 *Geology*, v. 33, p. 677-680.
- 847
- 848 Lisiecki, L.E., and Raymo, M.E., 2005, A Pliocene-Pleistocene stack of 57 globally distributed  
849 benthic  $\delta^{18}\text{O}$  records: *Paleoceanography*, v. 20, PA1003.
- 850
- 851 Linick, T.W., Jull, A.J.T., Toolin, L.J., and Donahue, D.J., 1986, Operation of the NSF-Arizona  
852 facility for radioisotope analysis and results from selected collaborative research projects:  
853 *Radiocarbon*, v. 28, p. 522-533.
- 854
- 855 Magee, J.W., Miller, G.H., Spooner, N.A., and Questiaux, D., 2004, Continuous 150 k.y.  
856 monsoon record from Lake Eyre, Australia: Insolation-forcing implications and  
857 unexpected Holocene failure: *Geology*, v. 32, p. 885-888.
- 858
- 859 McNeill, D.F., Klaus, J.S., O'Connell, L.G., Coates, A.G., and Morgan, W.A., 2013,  
860 Depositional sequences and stratigraphy of the Colón carbonate platform: Bocas Del  
861 Toro Archipelago, Panama: *Journal of Sedimentary Research*, v. 83, p. 183-195.
- 862
- 863 Milliman, J.D., 1974, *Marine carbonates: Recent sedimentary carbonates part 1*: Springer-  
864 Verlag, New York, Heidelberg, & Berlin, p. 375.
- 865
- 866 Milliman, J.D., 1995, Sediment discharge to the ocean from small mountainous rivers: The New  
867 Guinea example: *Geo-Marine Letters*, v. 15, p. 127-133.
- 868
- 869 Montaggioni, L.F., 2005, History of Indo-Pacific coral reef systems since the last glaciation:  
870 development patterns and controlling factors: *Earth-Science Reviews*, v. 71, p. 1-75.
- 871
- 872 Moss, P.T., and Kershaw, A.P., 2007, A late Quaternary marine palynological record (oxygen  
873 isotope stages 1 to 7) for the humid tropics of northeastern Australia based on ODP Site  
874 820: *Palaeogeography, Palaeoclimatology, Palaeoecology*, v. 251, p. 4-22.
- 875
- 876 Müller, G., and Gastner, M., 1971, The "Karbonat-Bombe", a simple device for the  
877 determination of the carbonate content in sediments, soils, and other materials: *Neues*  
878 *Jahrbuch für Mineralogie Monatshefte*, v. 10, p. 466-469.
- 879
- 880 Neil, D.T., Orpin, A.R., Ridd, P.V., and Bofu, Y., 2002, Sediment yield and impacts from river  
881 catchments to the Great Barrier Reef lagoon: *Marine Freshwater Research*, v. 53, p. 733-  
882 752.
- 883
- 884 Page, M.C., Dickens, G.R., and Dunbar, G.B., 2003, Tropical view of Quaternary sequence  
885 stratigraphy: siliciclastic accumulation on slopes east of the Great Barrier Reef since the  
886 Last Glacial Maximum: *Geology*, v. 31, no. 11, p. 1013-1016.

- Page, M.C. and Dickens, G.R., 2005, Sediment fluxes to Marion Plateau (southern Great Barrier Reef province) over the last 130 ky: new constraints on 'transgressive-shedding' off northeastern Australia: *Marine Geology*, v. 219, p. 27-45.
- Paul, A., Reijmer, J.J.G., Fürstenau, J., Kinkel, H., and Betzler, C., 2012, Relationship between Late Pleistocene sea-level variations, carbonate platform morphology and aragonite production (Maldives, Indian Ocean): *Sedimentology*, v. 59, p. 1640-1658.
- Peerdeman, F.M., and Davies, P.J., 1993, Sedimentological response of an outer-shelf, upper-slope sequence to rapid changes in Pleistocene eustatic sea level: Hole 820A, northeastern Australian margin: *Proceedings of the Ocean Drilling Program, Scientific Results*, v. 133, p. 303-313.
- Peerdeman, F.M., Davies, P.J., Chivas, A.R., 1993, The stable oxygen isotope signal in shallow-water, upper slope sediments off the Great Barrier Reef (Hole 820A): *Proceedings of the Ocean Drilling Program, Scientific Results*, v. 133, p. 163-173.
- Posamentier, H.W. and Allen, G.P., 1993, Variability of the sequence stratigraphic model: effects of local basin factors: *Sedimentary Geology*, v. 86, p. 91-109.
- Purdy, E.G., and Gischler, E., 2003, The Belize margin revisited: 1. Holocene marine facies: *International Journal of Earth Sciences*, v. 92, p. 532-551.
- Reimer, P.J., Bard, E., Bayliss, A., Beck, J.W., Blackwell, P.G., Bronk, R.C., Buck, C.E., Burr, Cheng, H., Edwards, R.L., Friedrich, M., Grootes, P.M., Guilderson, T.P., Hajdas, I., Hatté, C., Heaton, T.J., Hoffmann, D.L., Hogg, A.G., Hughen, K.A., Kaiser, K.F., Kromer, B., Manning, S.W., Niu, M., Reimer, R.W., Richards, D.A., Scott, E.M., Southon, Staff, R.A., Turney, C.S.M., van der Plicht, J., 2013, IntCal13 and Marine13 radiocarbon age calibration curves, 0-50,000 years cal BP: *Radiocarbon*, v. 55, p. 1869-1887.
- Rohling, E.J., Grant, K., Hemleben, C.H., Siddall, M., Hoogakker, B.A.A., Bolshaw, M., and Kucera, M., 2008, High rates of sea-level rise during the last interglacial period: *Nature Geoscience*, v. 1, p. 38-42.
- Sarg, J.F., 1988, Carbonate sequence stratigraphy, *in* Wilgus, C.G., Hastings, B.S., Ross, C.A., Posamentier, H.W., Van Wagoner, J.C., and Kendall, S.C., eds., *Sea-level Changes, an Integrated Approach: SEPM, Special Publication 42*, p. 155-181.
- Schlager, W. and Chermak, A., 1979, Modern sediment facies of platform-basin transition, Tongue of the Ocean, Bahamas, *in* Doyle, L. and Pilkey, O.H., eds., *Geological Continental Slopes: Special Publication, Soc. Econ. Paleontol. Mineral.*, v. 27, p. 193-208.
- Schlager, W., 1981, The paradox of drowned reefs and carbonate platforms, *GSA Bulletin*, v. 92,

p. 197-211.

Schlager, W., Reijmer, J.J.G., and Droxler, A.W., 1994, Highstand shedding of carbonate platforms: *Journal of Sedimentary Research*, v. 64, p. 270-281.

Shanmugam, G., and Moiola, R.J., 1983, Eustatic control of calciclastic turbidites: *Marine Geology*, v. 56, p. 273-278.

Slingerland, R., Driscoll, N.W., Milliman, J.D., Miller, S.R., and Johnstone, E.A., 2008, Anatomy and growth of a Holocene clinothem in the Gulf of Papua: *Journal of Geophysical Research*, v. 113, F01S13.

Tcherepanov, E.N., Droxler, A.W., Lapointe, P., Dickens, G.R., Benthley, S.J., Beaufort, L., Peterson, L.C., Daniell, J., and Opdyke, B.N., 2008, Neogene evolution of the mixed carbonate-siliciclastic system in the Gulf of Papua, Papua New Guinea: *Journal of Geophysical Research*, v. 113, F01S21, 21 p.

Thompson, P.R., Be, A.W.H., Duplessy, J., and Shackleton, N.J., 1979, Disappearance of pink-pigmented *Globigerinoides ruber* at 120,000 yr BP in the Indian and Pacific Oceans: *Nature*, v. 280, p. 554-557.

van der Plas, L., and Tobi, A.C., 1965, A chart for judging the reliability of point-counting results: *American Journal of Science*, v. 263, p. 87-90.

Vogt, C., 2009, Data report: semiquantitative determination of detrital input to ACEX sites based on bulk sample X-ray diffraction data, *in* Backman, J., Moran, K., McInroy, D.B., Mayer, L.A., and the Expedition 302 Scientists, *Proceedings IODP, 302: Edinburgh (Integrated Ocean Drilling Program Management International, Inc.)*. doi:10.2204/iodp.proc.302.203.2009 (12 pages). Open Access at IODP website Online since 05.05.2009.

Webster, J.M., Yokoyama, Y., Cotterill, C., and the Expedition 325 Scientists, 2011, *Proceedings, IODP, 325: Tokyo (Integrated Ocean Drilling Program Management International, Inc.)*. doi:10.2204/iodp.proc.325.2011.

Webster, J.M., Beaman, R.J., Puga-Bernabéu, Á., Ludman, D., Renema, W., Wust, R.A.J., George, N.P.J., Reimer, P.J., Jacobsen, G.E., and Moss, P., 2012, Late Pleistocene history of turbidite sedimentation in a submarine canyon off the northern Great Barrier Reef, Australia: *Palaeogeography, Palaeoclimatology, Palaeoecology*, v. 331-332, p. 75-89.

Wilson, J.L., 1967, Cyclic and reciprocal sedimentation in Virgilian strata of southern New Mexico: *Geological Society of America Bulletin*, v. 78, p. 805-818.

## Figures and Table

978  
 979 FIG. 1.---Maps of Great Barrier Reef and the Gulf of Papua showing land elevation and  
 980 bathymetry in the areas of Holes 58A, 820A, 819A and core MD-49. (A) overview of the entire  
 981 study area. (B) shelf and slope bathymetry at the locations of Holes 58A, 820A, and 819A along  
 982 the central GBR shelf and upper slope. (C) location of MD-49 on the upper slope of Ashmore  
 983 Trough with the northern GBR to the west, Ashmore Reef to the east, and the GoP shelf edge to  
 984 the north. Bathymetry combined and modified from GoP (Daniell 2008) and GBR-Coral Sea  
 985 (Beaman 2010) data sets.

986  
 987 FIG. 2.---Stratigraphic column at Hole 58A displaying individual cores, recovered intervals  
 988 (black), non-recovered intervals (crossed out white boxes), lithologic unit designation, grain size  
 989 (s = silt, vf = very fine sand, f = fine sand, m = medium sand, c = coarse sand, vc = very coarse),  
 990 Munsell color code, fabric, and nature of coarse grains. Units are described by grain size and  
 991 some grain type data sets are from this study, remainder from Proceedings of the IODP Volume  
 992 325 (Webster et al. 2011).

993  
 994 FIG. 3.---Hole 58A sediment physical properties in depth with lithologic units (Figure 2)  
 995 designated by alternating blue and white bands. Fine weight percent (red), carbonate content in  
 996 fine fraction (blue circles), light reflectance log (green circles), and magnetic susceptibility log  
 997 (black circles). Red dashed lines mark selected values separating high and low intervals of fine  
 998 weight percent, carbonate content, light reflectance, and magnetic susceptibility (see text).

999

FIG. 4.---Hole 58A; down-hole variations of carbonate content and mineralogy in addition to strontium counts from XRF core scans, blue and white bars identify the different lithologic units (Fig. 2), red dashed line defines our separation of relatively high and low values. Calcium carbonate trends and carbonate mineral trends: carbonate content (blue circles), strontium counts from XRF core scan (pink line) with overlying 5-pt mean (dark pink line), aragonite (light blue line), high-Mg-calcite (violet line), and calcite (dark blue line) from bulk XRD.

FIG. 5.---Hole 58A; down-hole variations of siliciclastics in depth, blue and white bars identify the lithologic units (Fig. 2), location of high and low intervals separation value (red dashed line). Siliciclastic mineralogy trends compared to carbonate content (blue circles): silica counts from XRF core scan (light orange line) with overlying 5-pt mean (dark orange line), quartz (light orange line), feldspar minerals (dark orange line), clay minerals (red line) from bulk XRD.

FIG. 6.---Correlation of Hole 58A Sr counts (XRF) and bulk aragonite percent (XRD). (A) Down-hole variations of Sr counts and aragonite. (B) Regression of aragonite percent versus Sr counts yield an  $R^2 = 0.8488$  and  $P\text{-value} = 3.69 \times 10^{-8}$ .

FIG. 7.---Depth and age conversion at Holes 58A, 820A, 819A, and core MD-49. Selected events on LR04 benthic stack (Lisiecki and Raymo 2005) are identified as tie-points along the oxygen isotope records of the studied holes and core. Marine isotope stage events are shown as labeled (name, age) red circles on LR04. Corresponding MIS events at Holes 58A, 820A, 819A, and core MD-49 (from Jorjy et al. 2010) as well as age tie points are shown in as labeled (name or age) red circles. Radiocarbon dates at Hole 58A shown as red diamonds. Radiocarbon dates

at Hole 820A from are shown as yellow diamonds with red outlines (see Peerdem and and Davies 1993 for dates). Occurrence of *Globigerinoides ruber* (pink variety) is shown at Hole 58A, Hole 820A (Peerdeman et al. 1993), Hole 819 (from Alexander et al. 1993, with a transitional and not sharp disappearance level), and core MD-49 (Jorjy et al. 2010) as a shaded pink area.

FIG. 8.---Variation of oxygen isotopes at Holes 58A, 820A, 819A, and core MD-49 compared with LR04 benthic stack. Hole 58A oxygen isotope record, in red, overlays MD-49 to demonstrate close fit of the two records. Interglacial and glacial/interstadial marine isotope stages (Lisiecki and Raymo 2005) are displayed as blue and grey bands respectively.

FIG. 9.---Hole 58A sediment physical properties displayed in time with, in the background, interglacial and glacial marine isotope stages (Lisiecki and Raymo 2005) shown as blue and grey intervals, respectively (see Fig. 8). Data plotted: fine weight percent (red), carbonate content (blue circles) from fine fraction, light reflectance log (green circles), and magnetic susceptibility log (black circles). Dashed red dashed line denotes value used for separation of high and low intervals (see text).

FIG. 10.---Variation in time of carbonate content at Holes 58A, 820A, 819A, and core MD-49 plotted with each respective oxygen isotope record (pink lines). In the background, interglacial and glacial marine isotope stages (Lisiecki and Raymo 2005) designated by blue and grey (see Fig. 8).



FIG. 11.---Comparison of mass accumulation rates ( $MAR - g \cdot cm^{-2} \cdot ky^{-1}$ ) at Holes 58A, Hole 820A, and MD-49 (Jorjy et al. 2010) from 150 – 75 ka. KL11+1017 Red Sea sea level curve (Rohling et al. 2009) is shown as a dashed pink line, carbonate MAR (blue line), siliciclastic MAR (red line), and aragonite MAR (green line) displayed for each studied hole and core location, when available. Hole 820A MAR data calculated from carbonate content and density data from Peerdeman et al. (1993).

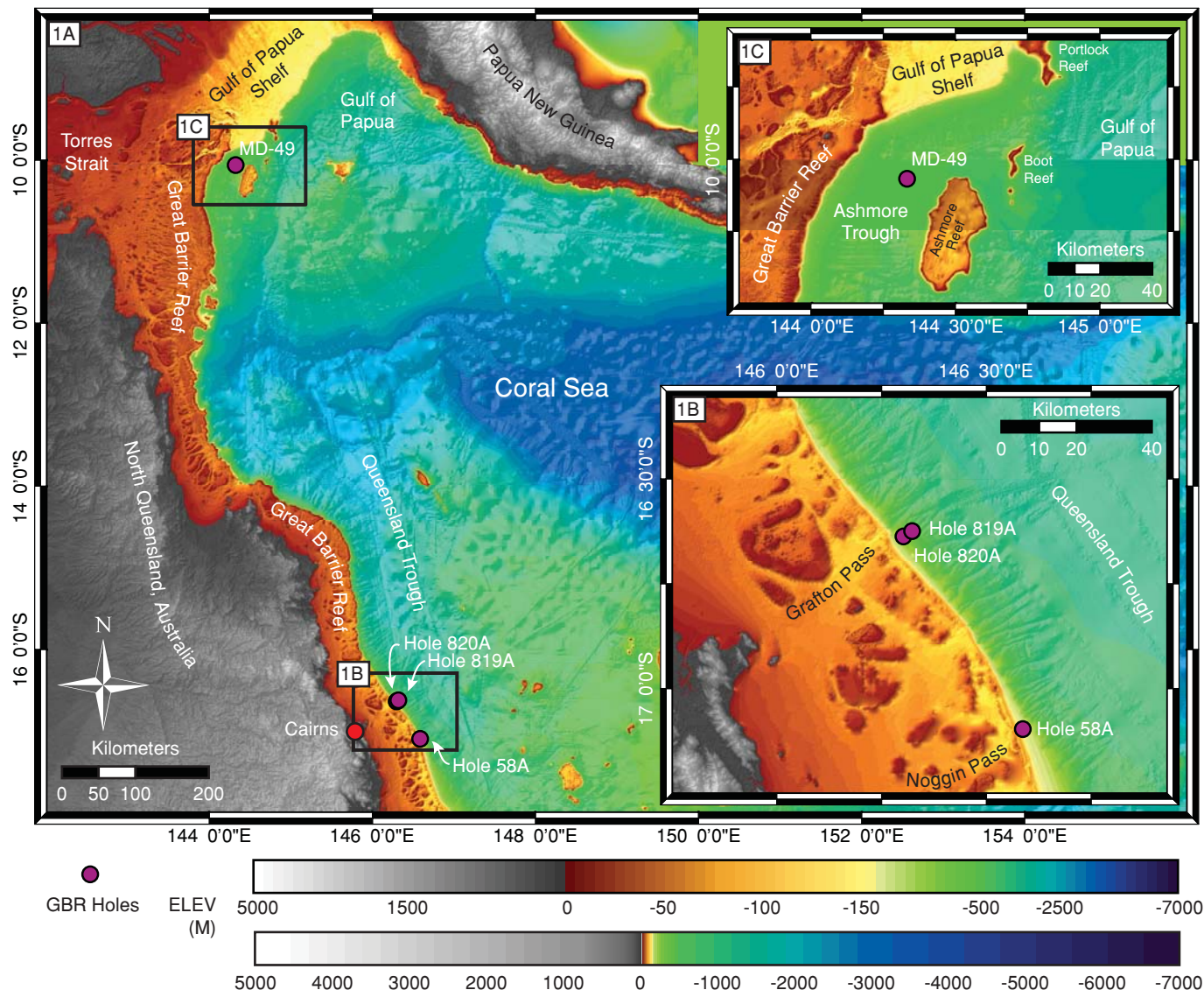
FIG. 12.---Comparison of mass accumulation rates ( $MAR - g \cdot cm^{-2} \cdot ky^{-1}$ ) and strontium counts from XRF core scans at Hole 58A and MD-49 (Jorjy et al. 2010; Sr counts from Kazuyo Tachikawa, Personal Communication) for a time interval spanning 145 – 100 ka, including Termination II and MIS-5e to 5d, blue background is MIS-5e and grey background is MIS-6. Hole 58A MAR aragonite (dark blue), Hole 58A strontium (light blue), MD-49 MAR aragonite (Red), MD-49 strontium (orange), with KL11+1017 sea level curve (Rohling et al. 2009) shown as a black dashed line.

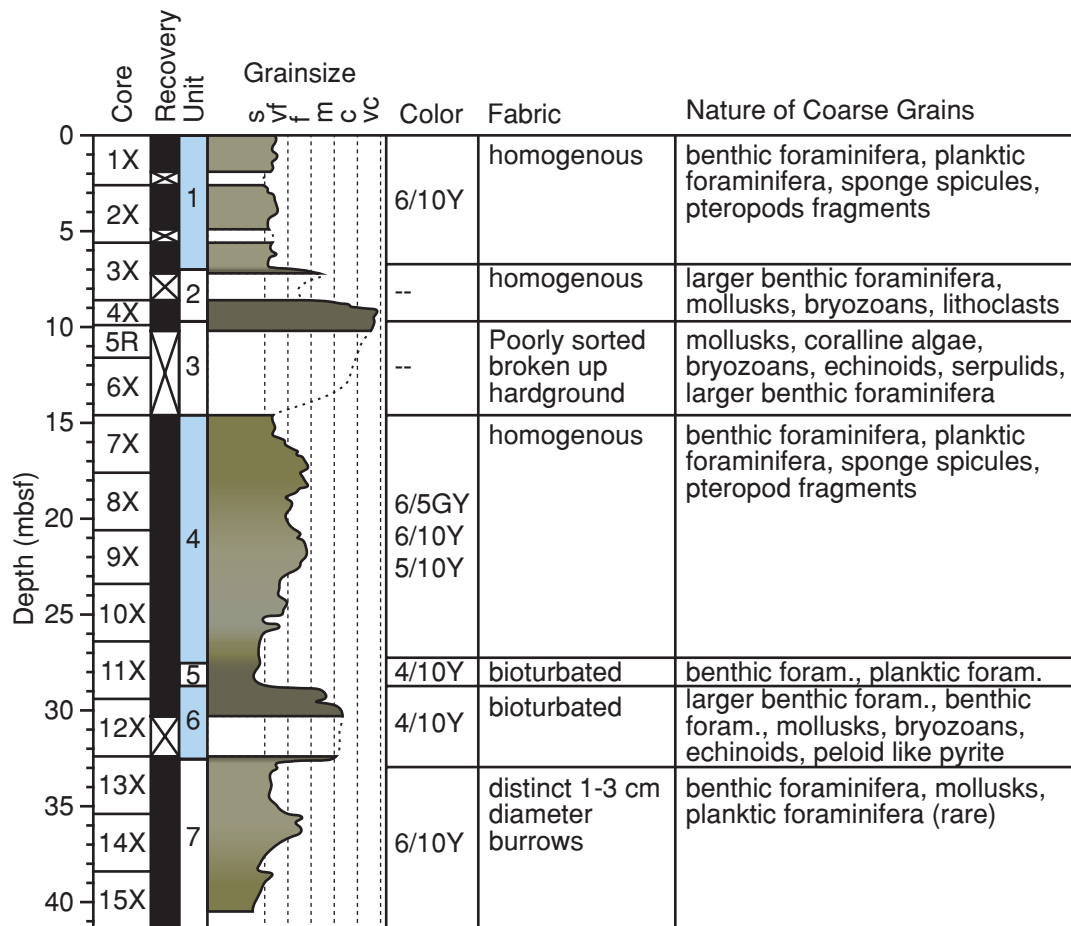
FIG. 13.---Conceptual models for environmental change on the central Great Barrier Reef shelf and sediment transport variation to the upper slope during the penultimate glacial-interglacial cycle from MIS-6 to MIS-5a. Green rectangle shows sea level (Rohling et al. 2009) conditions at each time interval. (A) Glacial: late MIS-6, low sea level exposes shelf. (B) Deglaciation: Termination II, MIS-6/5 a transition with sea level rising. (C) Peak interglacial: MIS-5e when shelf is completely re-flooded and the GBR is mostly drowned. (D) Late Interglacial: MIS-5d to 5a interval of falling sea level and re-entry of reef substrate into the euphotic zone.

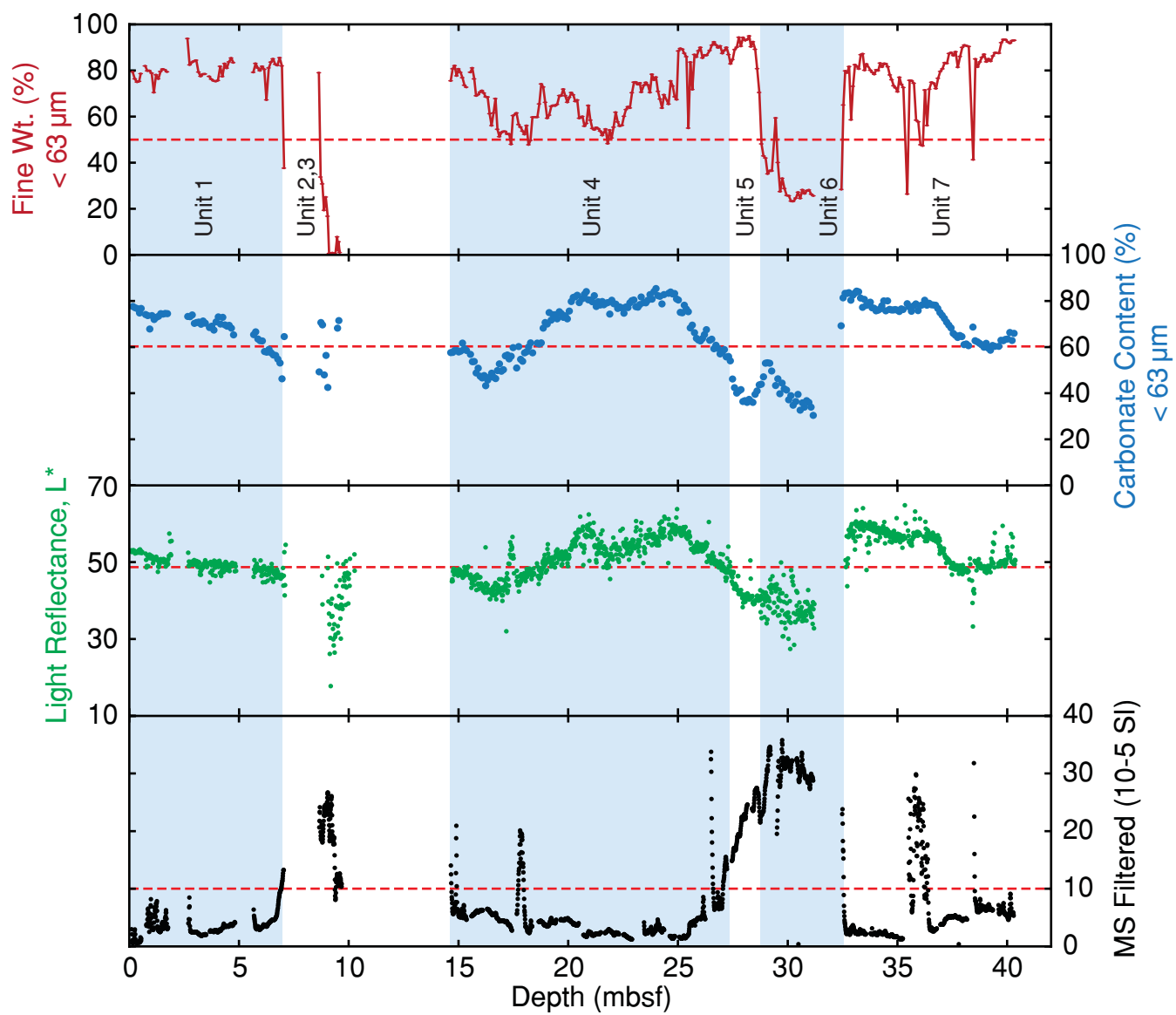
1069 Table 1.---Composition of three grainstone-packstone samples from Unit 2 at Hole 58A,  
1070 including: grain nature, bulk mineralogy, and cement mineralogy.

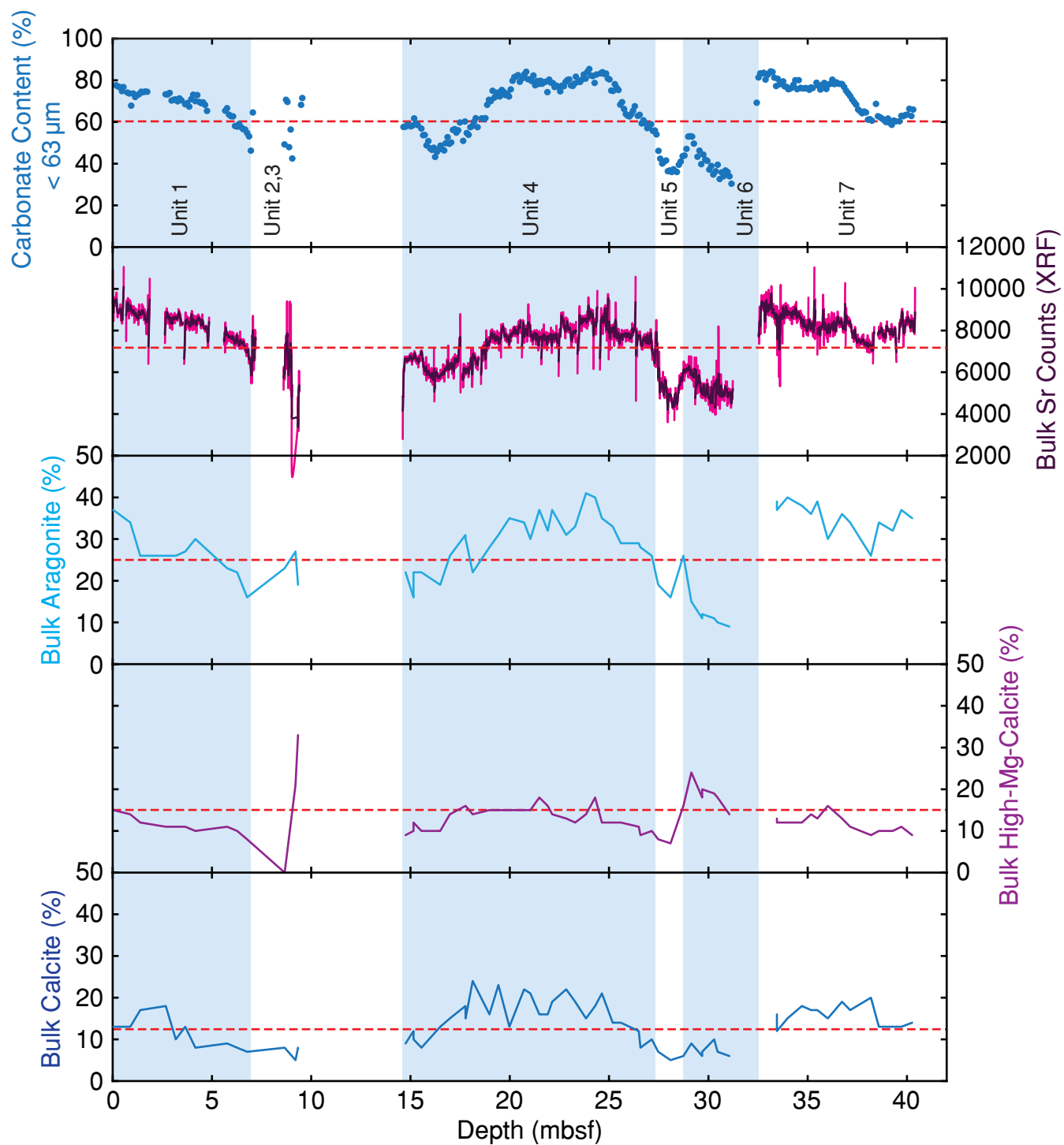
1071

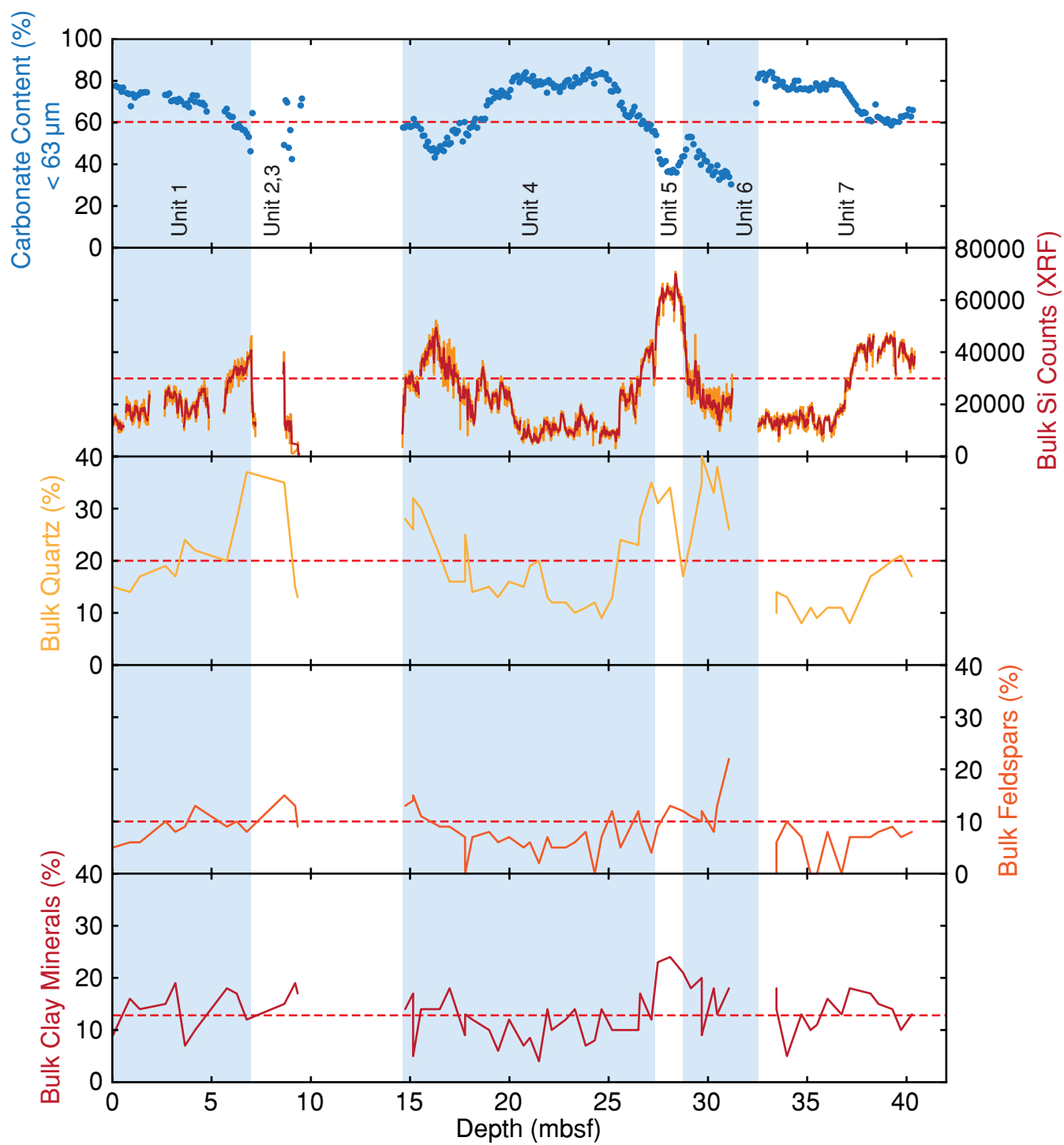
1072 Table 2.---Hole 58A chronostratigraphic tie points based on marine isotope stage events used to  
1073 create age depth model with associated depth age plot implying sedimentation rates.

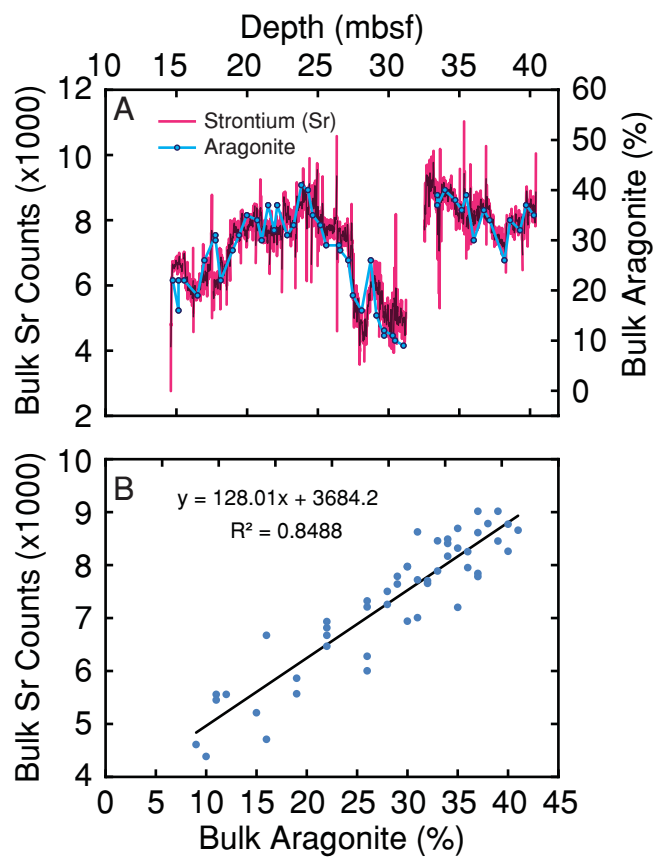




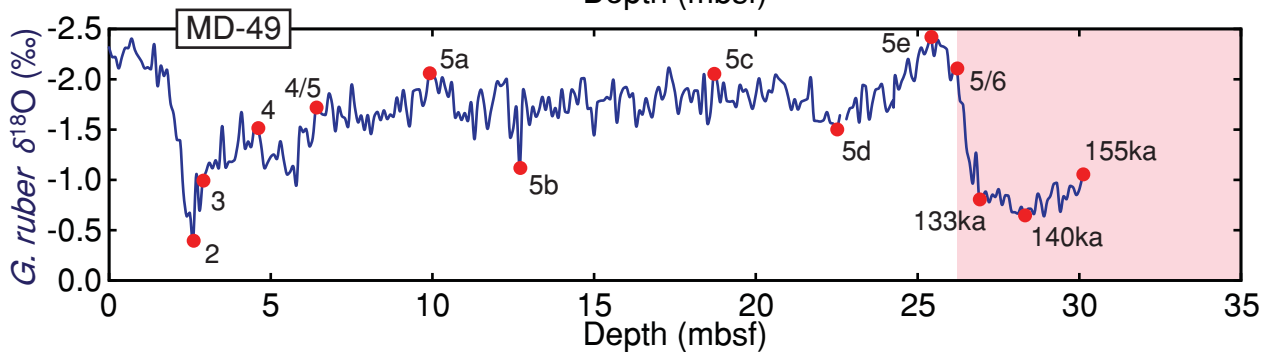
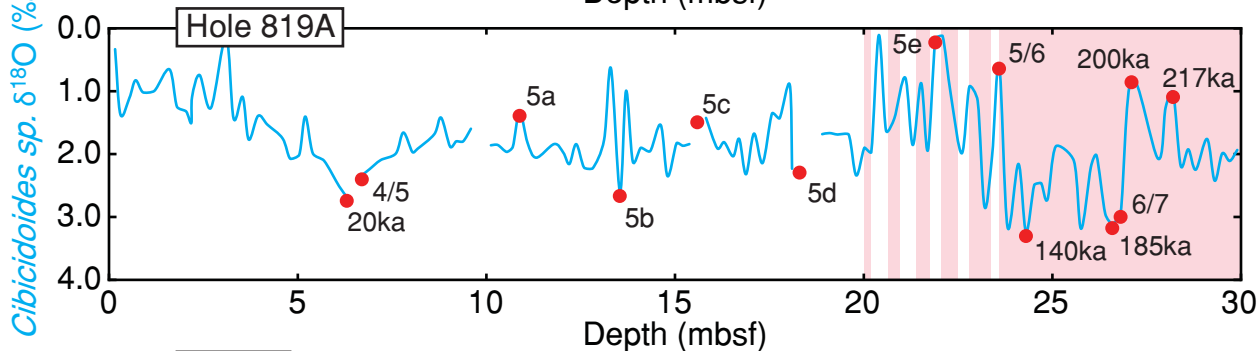
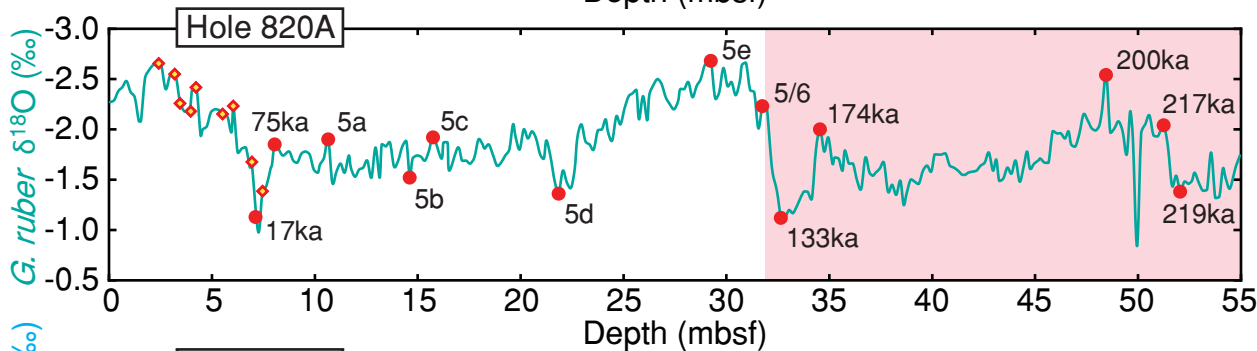
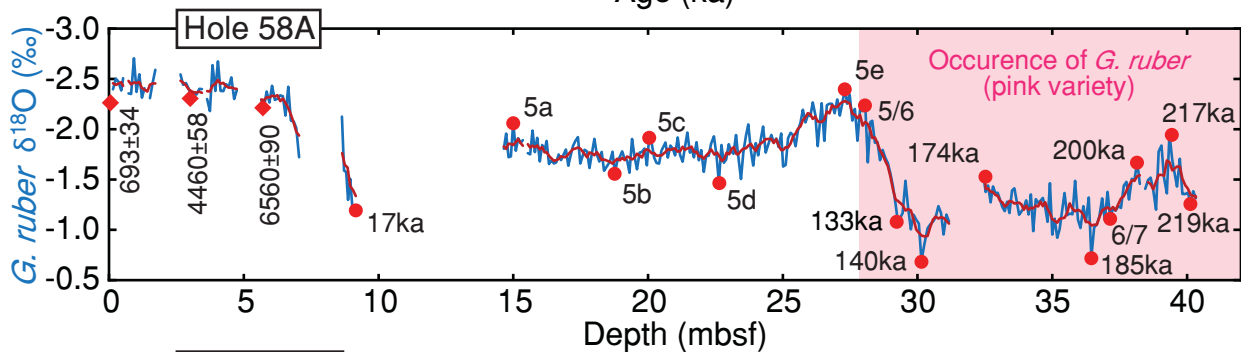
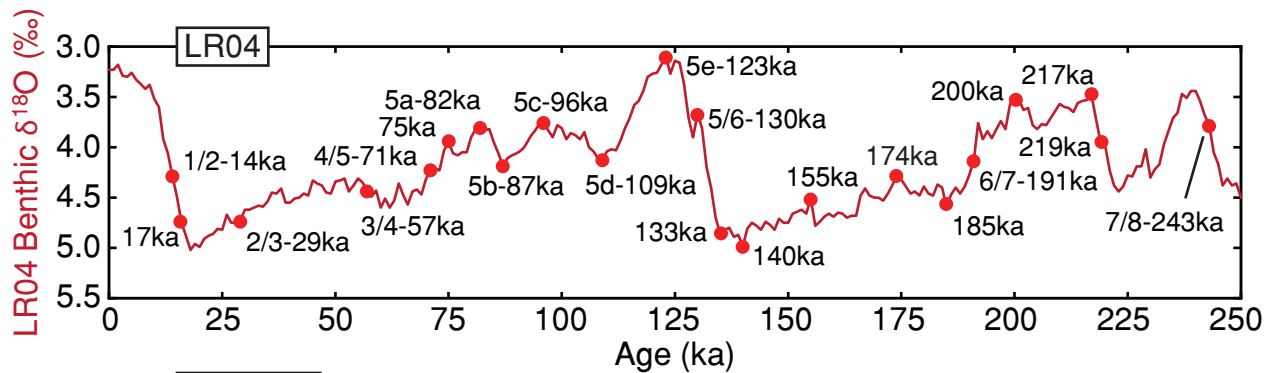


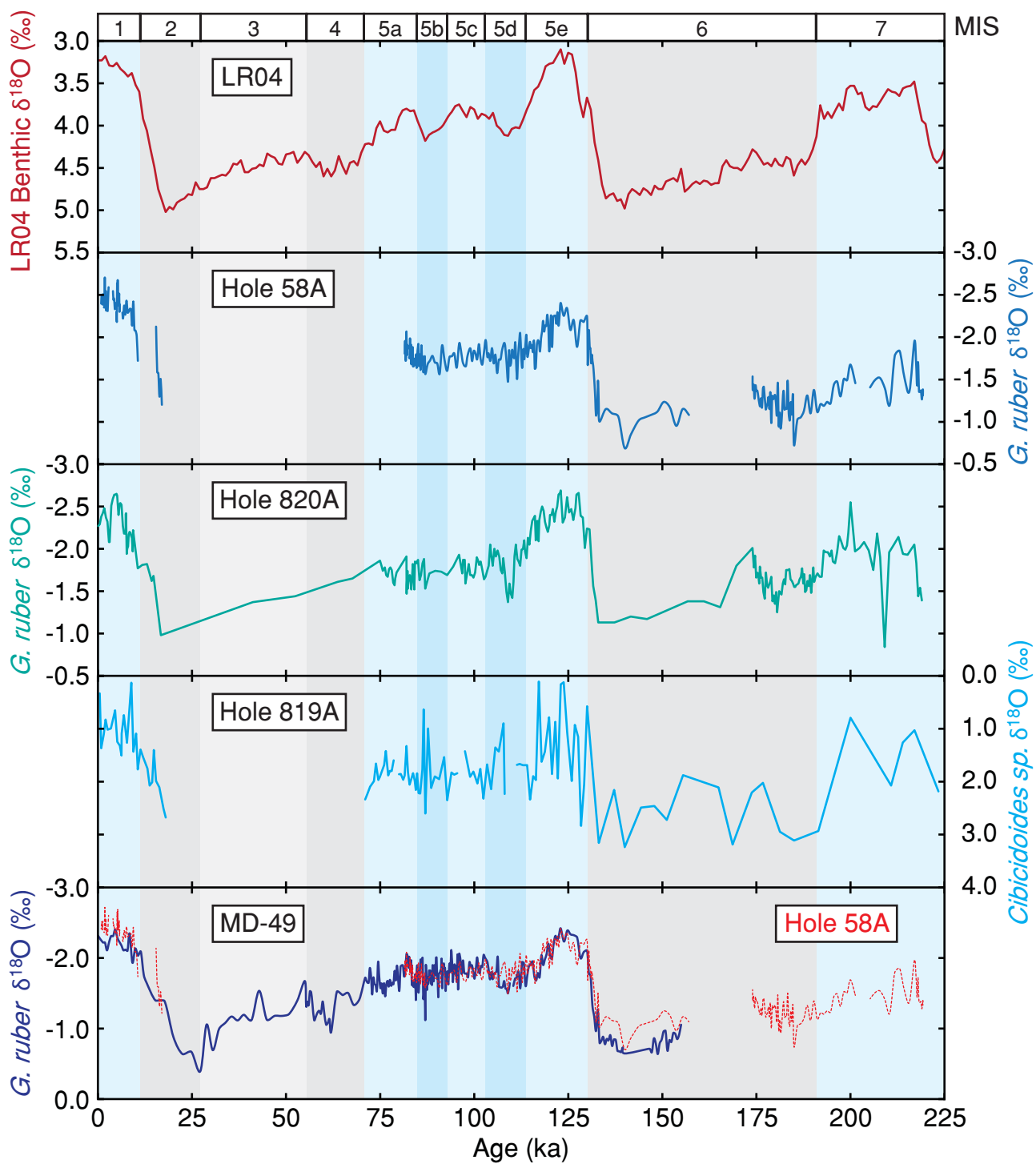


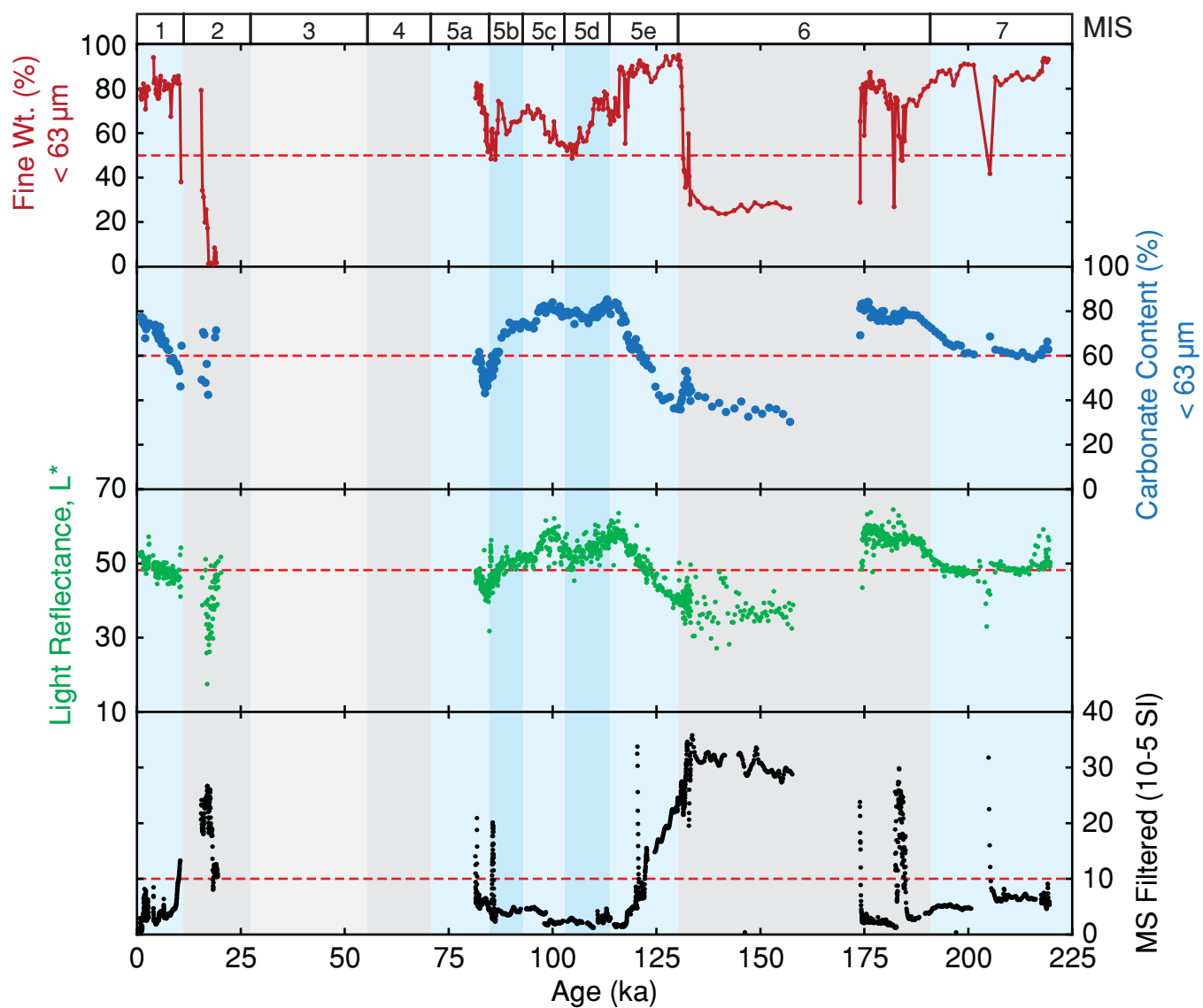


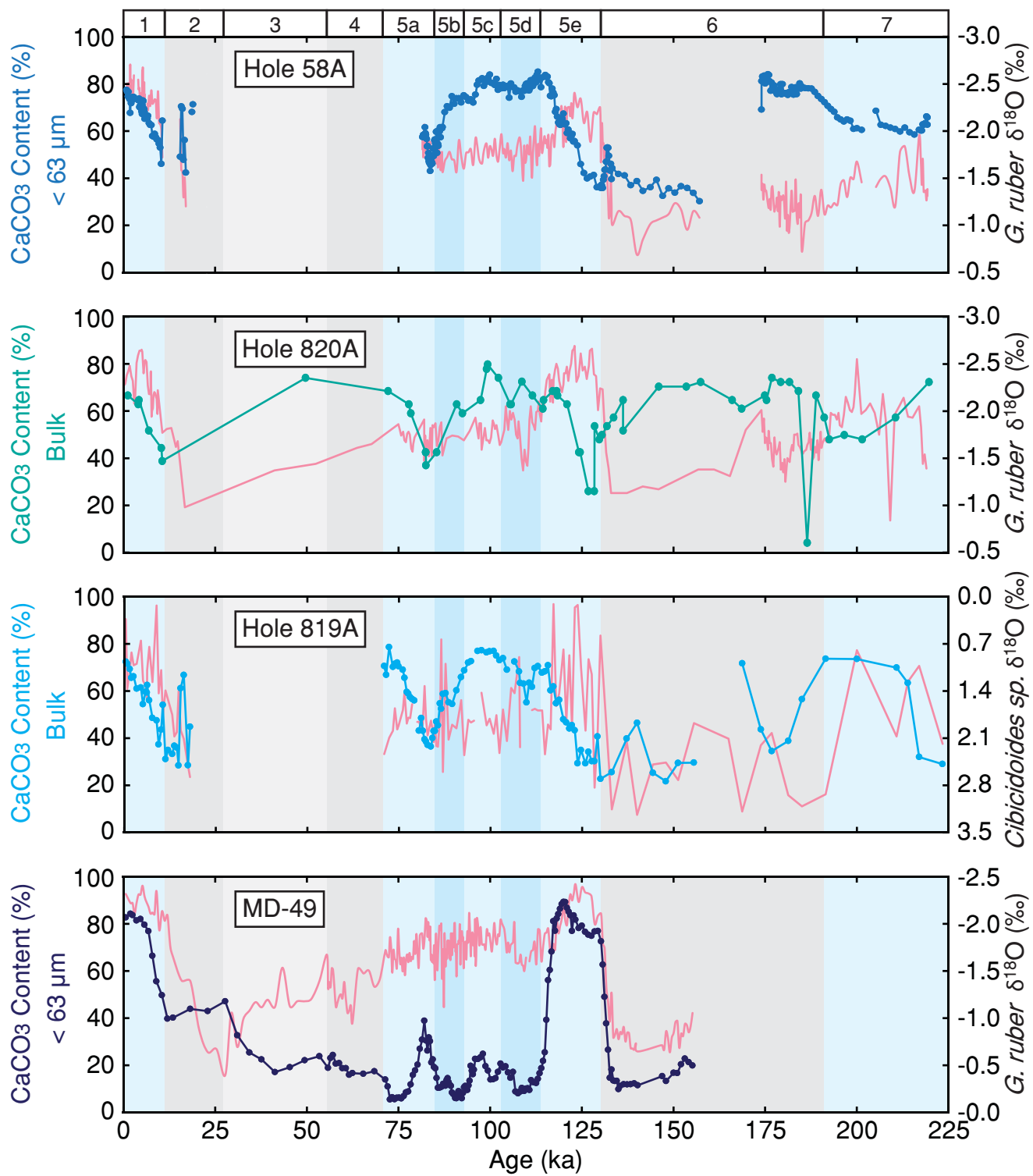


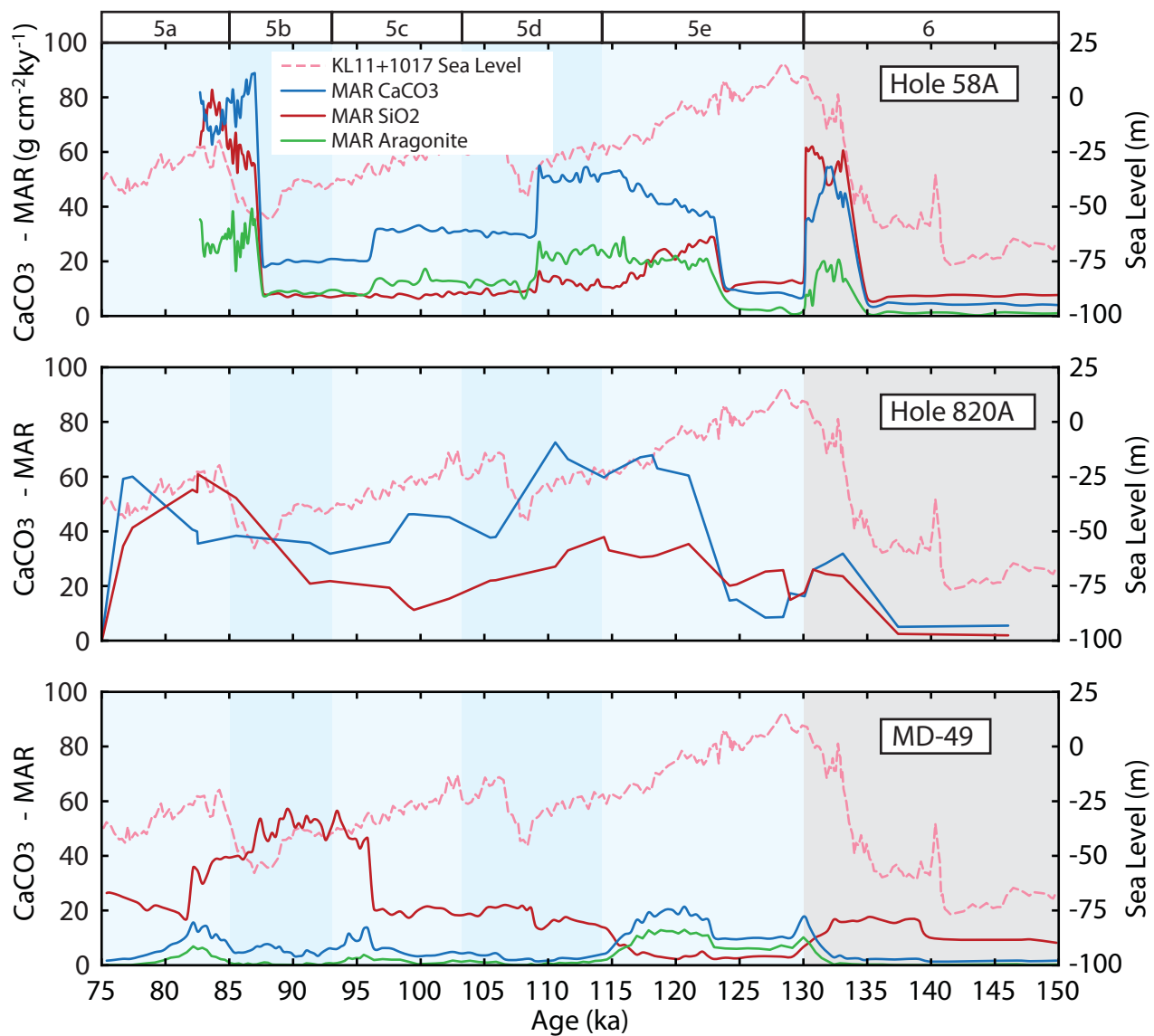


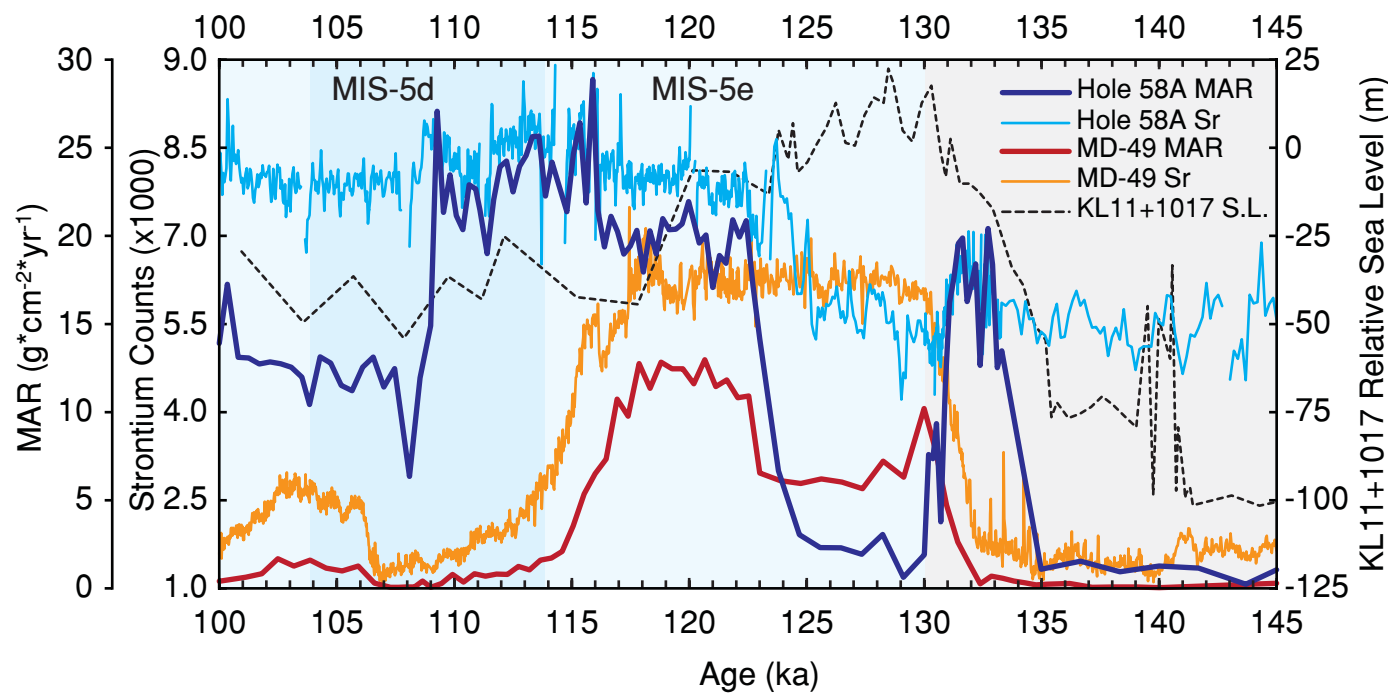




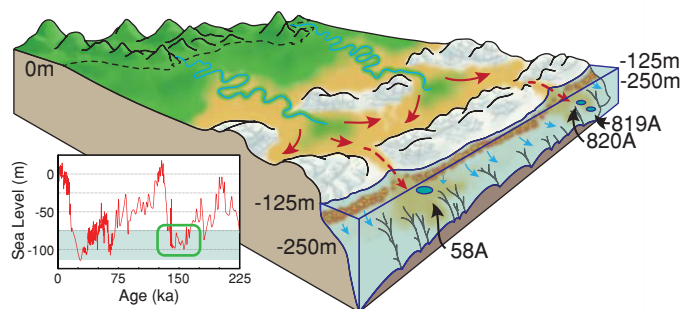






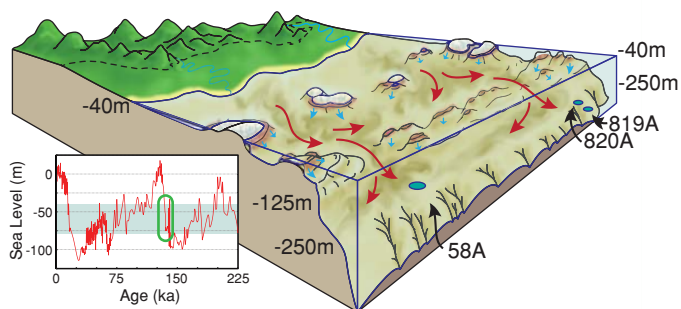


### 13A - Glacial: Late MIS-6



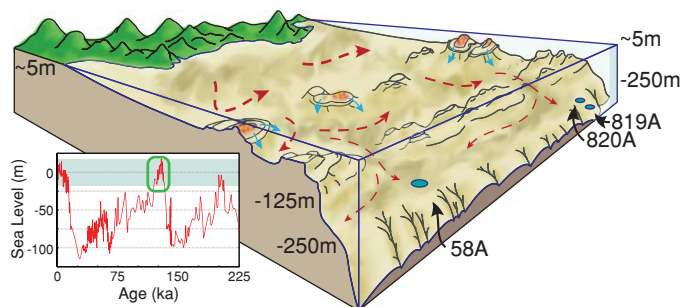
Minimum sea level, GBR shelf exposed and reefs undergoing karstification. Terrigenous material accumulates within a broad coastal plain between reef mounds with little shelf bypass. Fringing reefs contribute coarse carbonate material to the upper slope that is cemented by high-Mg-calcite.

### 13B - Deglaciation: MIS-6/5a Transition



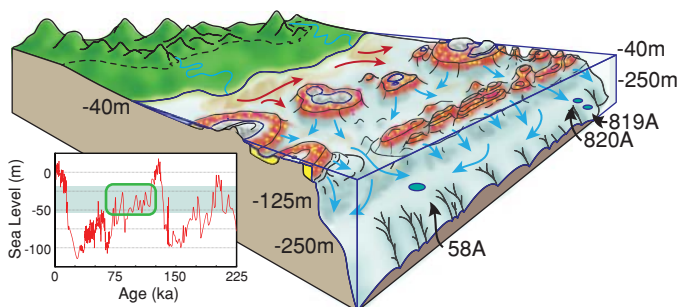
Rising sea level, GBR shelf re-flooded resulting in the formation of insipient reefs and the reworking and transport of fine siliciclastic material and to the upper slope.

### 13C - Peak Interglacial: MIS-5e



Maximum sea level, GBR shelf fully flooded. Rapid sea level rise drowns incipient reefs. Small amounts of very fine siliciclastic material is transported to the upper slope. Sedimentation rates are minimal for both siliciclastic and carbonate material.

### 13D - Late Interglacial: MIS-5d to 5a



Falling sea level, high relief areas on the GBR shelf re-enter the euphotic zone and the carbonate factory is reactivated, exporting fine carbonate material to the upper slope. Siliciclastic material is largely restricted to the coastal region.



Table 1. Lithoclast Composition

Sample		Coarse Grains (%)							
Core, Interval	coral	coralline Algae	<i>Halimeda</i>	mollusk	benthic foram	planktic foram	echinoderm	bryozoa	quartz
4X-1, 65.0-69.0 cm	2.7	4.7	5.0	20.7	17.0	2.7	5.0	13.3	3.0
4X-1, 84.0-88.0 cm	0.3	2.3	2.7	24.0	20.0	3.7	1.7	4.7	3.7
4X-1, 98.5-102.5 cm	1.3	8.0	2.3	15.7	19.3	5.0	1.3	12.7	0.7
MEAN	1.4	5.0	3.3	20.1	18.8	3.8	2.7	10.2	2.5
Porosity and Cement (%)								Sum (%)	
	primary porosity	secondary porosity	micrite env.	needle cement	peloidal cement	microcrystal cement	sediment ("matrix")	Grains, Porosity, Cement	
4X-1, 65.0-69.0 cm	9.3	0.3	2.0	3.0	6.3	5.0	0.0	100.0	
4X-1, 84.0-88.0 cm	6.7	0.6	1.7	4.7	10.0	5.0	8.3	100.1	
4X-1, 98.5-102.5 cm	8.0	1.3	0.3	7.7	14.0	0.3	2.0	99.9	
MEAN	8.0	0.7	1.3	5.1	10.1	3.4	3.4	100.0	
Mineralogy and Bulk Carbonate Composition									
	aragonite	HMC	LMC	carbonate	insoluble Residue				
	wt.-%	wt.-%	wt.-%	%	%				
4X-1, 65.0-69.0 cm	33.7	55.8	10.5	90.0	10.0				
4X-1, 84.0-88.0 cm	39.4	49.8	10.8	94.0	6.0				
4X-1, 98.5-102.5 cm	43.9	48.9	7.3	98.0	2.0				
MEAN	39.0	51.5	9.5	94.0	6.0				



Table 2. Chronology Tie Points

